Electromechanical Energy Conversion in Asymmetric Piezoelectric Bending Actuators

Vom Fachbereich Mechanik
der Technischen Universität Darmstadt
zur Erlangung des Grades eines
Doktor-Ingenieurs (Dr.-Ing.)
genehmigte

Dissertation

von

Dipl.-Ing. Kai-Dietrich Wolf

aus Wiesbaden

Referent:	Prof. Dr. P. Hagedorn
Korreferent:	Prof. Dipl.-Ing. Dr. techn. H. Irschik
Tag der Einreichung:	26.04.2000
Tag der mündlichen Prüfung:	29.05.2000

Darmstadt 2000
D 17

Vorwort

Die vorliegende Arbeit entstand während meiner Tätigkeit als wissenschaftlicher Mitarbeiter bei Prof. Dr. P. Hagedorn in der Arbeitsgruppe Dynamik des Fachbereichs Mechanik der Technischen Universität Darmstadt.

An erster Stelle möchte ich mich bei Herrn Professor Hagedorn bedanken für die Anregung zu dieser Arbeit und die durch seine Persönlichkeit gesetzten akademischen und menschlichen Rahmenbedingungen, die das Arbeiten in dieser Gruppe überaus angenehm machten. Herrn Professor Irschik gilt mein Dank für die bereitwillige und sehr wohlwollende Übernahme des Korreferats.

Besonders herzlich bedanke ich mich bei meinen ehemaligen Kolleginnen und Kollegen, Frau Jutta Braun und Frau Renate Schreiber, den Herren Dipl.-Ing. Thomas Sattel, Marcus Berg, Daniel Sauter, Georg Wegener, Hartmut Bach, Norbert Skricka, Roland Platz, Malte Seidler, Uli Ehehalt, den Herren Dr.-Ing. Minh Nam Nguyen, Joachim Schmidt, Ulrich Gutzer, Thomas Hadulla, Karl-Josef Hoffmann, Dirk Laier, Utz von Wagner, Christoph Reuter und Herrn Prof. Dr.-Ing. Wolfgang Seemann für Ihre Hilfsbereitschaft und stetige Anteilnahme.

Ein wesentlicher Teil dieser Arbeit wurde von meinen Diplomarbeitern, den Herren Dipl.-Ing. Stephan Frese und Boris Stöber mitgeleistet. Ihnen danke ich für ihren Fleiß und die sehr freundschaftliche Zusammenarbeit.

Die Herren Professoren A.F. Ulitko und Oleg Yu. Zharii haben durch ihre Anregungen dieser Arbeit wesentliche Impulse gegeben. Auch für die mir entgegengebrachte menschliche Nähe möchte ich ihnen an dieser Stelle besonders danken.

Darmstadt, im Juni 2000

Kai Wolf

Contents

Chapter 1

Introduction

1.1 Motivation

Among the various wave types in solid structures, bending waves are associated with the largest deflections. Consequently, most of the mechanical interaction with the surrounding environment, e.g. sound radiation, is to be accounted to the bending or flexural deformation [CH88], typically observed in plate or beam structures which are characterized by a small thickness compared to longitudinal dimensions. The large attainable deflections and the resulting potential for mechanical interaction is the motivation to control flexural waves in beams and plates. Control strategies are often implemented in electronic circuits or microprocessors and the power required to control the structure will most likely be provided electrically. Generally, actuators are the means required to convert the electrical power supplied into any form of mechanical power. Ideally, the mechanical actuation would be suitable to enforce control authority over all flexural waves in the structure. In structures containing beam or plate members, this requires several distributed low authority actuators rather than a single one with high control authority and structures with integrated distributed actuators are often referred to as *intelligent* or *smart structures* [CDL87]. Patches of piezoelectric ceramics, which can easily be bonded to the surface of beams or plates, have proven to be well suited to serve as actuators to control flexural vibrations and optimization of the design [KJ91] of these patches for this purpose has been a concern.

In high power applications, such as ultrasonic traveling wave motors, where piezoceramic layers are employed for continuous energy transfer [UTKN93], the power flow and thus the maximum power output of the motor is limited by saturation effects. Actuators should be designed in a way that critical field variables are kept as small as possible. Power loss, which can be caused by a variety of loss mechanisms in the actuator, leads to undesired heat production. Material properties of the piezoelectric material are temperature sensitive and excessive heat can even cause permanent depolarization. Therefore, the design of the piezoelectric bending actuator should be carefully considered to provide optimal energy conversion.

1.2 Scope of this Work

Once the need for optimization is recognized, the first question to ask is: what is optimal? The more details about the particular structure are known, the more comprehensive but also complex can the mathematical model be and analytical solutions will generally not be available. In the case of the ultrasonic traveling wave motor, energy is transferred between rotor and stator by a highly nonlinear friction mechanism which defies detailed analytical treatment. An optimization criterion would ideally be independent of such detailed modeling and still give authoritative guidelines for the design of the actuator.

This work aims at a general consideration of energy conversion in bending actuation rather than detailed modeling of particular systems. *Energy conversion will be considered good if a large fraction of the electrical work supplied to the system is converted into mechanical work and vice versa, where it is acknowledged that energy conversion has to be carried out in cycles.* It will be shown that the electromechanical coupling factor (EMCF) and the actuator power factor are measures which comply with this definition, based on a hypothetical quasi-static work cycle or harmonic steady state vibration, respectively. In spite of the fact that power actuators are most likely operated in the regime of nonlinear material behavior, the analysis carried out is confined to the domain of linear equations. This restriction is due to the difficulties arising in the analytical treatment of nonlinear material behavior in continuous systems. It is anticipated here, that an optimization of the energy conversion based on linear assumptions will lead to an overall reduction of field intensities in the piezoelectric material and thus increase the attainable power flow and reduce the power loss due to various loss mechanisms.

Chapter 2

Piezoelectric Ceramics

2.1 A Model for Piezoelectric Solids

The term *'dielectric solid'* in this work is used for a continuous elastic body with dielectric properties, which constitute the interaction between the electrical quantities dielectric displacement and electric field. As in the case of the elastic interaction between strain and stress it is assumed that the dielectric interaction is free of loss mechanisms. A dielectric solid which also exhibits lossless interaction between electrical and mechanical quantities will be referred to as piezoelectric solid, so piezoelectric solids represent a subset of the dielectric solids. The absence of loss implies that the state of the system is uniquely determined by the independent state variables, regardless of the path taken in state space. Feasible paths can mathematically be determined as solutions to the equations of motion.

An elegant method to obtain the equations of motion is the use of variational principles, which also have certain advantages when complicated boundary conditions are to be treated. For piezoelectric solids, HAMILTON's principle is frequently employed and instead of the internal energy U which is used for mechanical problems, the *electric enthalpy* H is substituted into the LAGRANGEian. Many authors refer to TIERSTEN [Tie69], who probably coined the name 'electric enthalpy', to explain the origin of this expression, but no satisfactory derivation can be found in this reference. Variational methods for piezoelectric solids were presented by TIERSTEN, HOLLAND and EER NISSE earlier [Tie68], [HN68],

[Nis67], but there it is rather demonstrated that the requirement of a particular energy expression to be stationary leads to the balance equations, than how to arrive at the electric enthalpy H and a corresponding expression for the virtual work for substitution into Hamilton's principle. Therefore, a brief derivation of Hamilton's principle shall be given and it will be seen that the electric enthalpy density H but also the energy density U can be substituted into the Lagrangeian, provided a corresponding expression for the virtual work is used.

2.1.1 A derivation of Hamilton's principle for dielectric solids

The balance of momentum for a continuum can be written as

$$T_{ij,j} + F_i = \frac{\mathrm{d}}{\mathrm{d}t}(\rho \dot{u}_i), \tag{2.1}$$

where T_{ij}, F_i and $\dot{u}_i$ are the components of the stress tensor, the force per unit volume and the velocity, respectively, and ρ is mass per unit volume. For the applications considered in this work, interaction between electrical quantities can be treated as quasistatic [Mau88], [Aul81], so magnetic field effects can be neglected and Maxwell's equations reduce to

$$D_{k,k} = \rho_\mathrm{f}, \tag{2.2}$$

$$E_k = -\phi_{,k}, \tag{2.3}$$

for the electric displacement D_k and the electric field E_k, which can be represented by the negative gradient of the electric potential ϕ. Here, the comma indicates differentiation with respect to the orthogonal cartesian coordinates x_i , $(i = 1, 2, 3)$. Inside the electrically insulating dielectric, free charges do not exist and the free charge density per unit volume ρ_f in (2.2) is zero. However, free charges will exist on the electroded surfaces of the dielectric.

The above equations of equilibrium (2.1)-(2.3) hold at any point of a continuum[1)] and from now on, a volume fraction of this continuum which is occupied by the dielectric solid, having volume V, is considered. On the surface S of the solid, mechanical and electrical boundary conditions apply. Mechanical boundary conditions will be given on the distinct sections S_u, S_f of the surface either in terms of prescribed displacement

$$u_i = \bar{u}_i \quad \text{on} \quad S_u, \tag{2.4}$$

[1)] Provided, that the quasistatic approximation is justified, of course.

or prescribed force per unit area

$$T_{ij}n_j = \bar{f}_i \quad \text{on} \quad S_f, \tag{2.5}$$

where n_j is the outward normal unit vector and $S_u \cup S_f = S$. Correspondingly, electrical boundary conditions are either prescribed surface charge density

$$-D_i n_i = \bar{\sigma} \quad \text{on} \quad S_\sigma, \tag{2.6}$$

or prescribed potential

$$\phi = \bar{\phi} \quad \text{on} \quad S_\phi, \tag{2.7}$$

and $S_\phi \cup S_\sigma = S$. The free charges on the surface electrodes can be represented by a density σ of charge per unit surface, if the thickness of the electrode is negligible. This, and the assumption that the dielectric displacement on the outside of the dielectric body is small compared to the inside in connection with (2.2), leads to (2.6).

In a similar way as it can be done for a purely mechanical system [Was68], a variational principle can be derived from the equations of equilibrium (2.1)-(2.3) and boundary conditions (2.4)-(2.7). After multiplication by the variation $\delta u_i, \delta\phi$ of the quantities u_i, ϕ and integration over the volume and surface of the body, a weak form

$$\begin{aligned} - & \int_V \left[T_{ij,j} + F_i - \frac{\mathrm{d}}{\mathrm{d}t}(\rho \dot{u}_i) \right] \delta u_i \,\mathrm{d}V + \int_{S_f} (T_{ij}n_j - \bar{f}_i)\delta u_i \,\mathrm{d}S \\ - & \int_V D_{k,k}\delta\phi \,\mathrm{d}V + \int_{S_\sigma} (D_i n_i + \bar{\sigma})\delta\phi \,\mathrm{d}S = 0 \end{aligned} \tag{2.8}$$

of the problem (2.1)-(2.7) is obtained. Here, the choice of the signs of the integral expressions in (2.8) is arbitrary, but in this form particularly suitable for the further derivation. The variations $\delta u_i, \delta\phi$ are chosen to satisfy the displacement and potential boundary conditions, i.e. they vanish on S_u and S_ϕ, respectively. Partial integration and application of the divergence theorem lead to

$$\begin{aligned} & \int_V (T_{ij}\delta S_{ij} - D_k \delta E_k) \,\mathrm{d}V - \int_V \left[F_i - \frac{\mathrm{d}}{\mathrm{d}t}(\rho \dot{u}_i) \right] \delta u_i \,\mathrm{d}V \\ + & \int_{S_\sigma} \bar{\sigma}\delta\phi \,\mathrm{d}S - \int_{S_f} \bar{f}_i \delta u_i \,\mathrm{d}S = 0, \end{aligned} \tag{2.9}$$

where the linear strain tensor

$$S_{ij} = \frac{1}{2}(u_{i,j} + u_{j,i}) \tag{2.10}$$

has been introduced, assuming that only small deformations are encountered.

If only contributions of the mechanical and electrical quantities to the energy of the system are considered, the total differential

$$\mathrm{d}U = T_{ij}\,\mathrm{d}S_{ij} + E_k\,\mathrm{d}D_k \tag{2.11}$$

of the internal energy density U, shows that U is a function of the independent variables strain S_{ij} and dielectric displacement D_k. Let another energy expression, the electric enthalpy density H [TIE69], be defined as

$$H = U - E_k D_k, \tag{2.12}$$

which is obtained from U by a LEGENDRE transformation. Since

$$\mathrm{d}H = T_{ij}\,\mathrm{d}S_{ij} - D_k\,\mathrm{d}E_k, \tag{2.13}$$

H is a function of the independent variables strain S_{ij} and electric field E_k which in turn are functions of u_i and ϕ, respectively. If the volume forces F_i vanish and ρ is independent of time, (2.9) can be written

$$\int_V \delta H\,\mathrm{d}V + \int_V \rho\frac{\mathrm{d}}{\mathrm{d}t}(\dot{u}_i)\delta u_i\,\mathrm{d}V + \int_S (\bar{\sigma}\delta\phi - \bar{f}_i\delta u_i)\,\mathrm{d}S = 0, \tag{2.14}$$

and further partial integration over time between t_1 and t_2 leads to

$$\int_{t_1}^{t_2}\int_V \left[\delta H - \frac{1}{2}\rho\,\delta(\dot{u}_i^2)\right]\,\mathrm{d}V\,\mathrm{d}t + \int_{t_1}^{t_2}\int_S (\bar{\sigma}\delta\phi - \bar{f}_i\delta u_i)\,\mathrm{d}S\,\mathrm{d}t = 0, \tag{2.15}$$

requiring the variations δu_i and $\delta\phi$ to vanish at t_1, t_2. With the LAGRANGEian

$$L = \int_V (\frac{1}{2}\rho\dot{u}_i^2 - H)\,\mathrm{d}V = \int_V (T - H)\,\mathrm{d}V, \tag{2.16}$$

where T denotes kinetic energy density of the body, and the virtual work of the given forces $\bar{f}_i$ and charges $\bar{\sigma}$

$$\delta W = \int_S (\bar{f}_i\delta u_i - \bar{\sigma}\delta\phi)\,\mathrm{d}S, \tag{2.17}$$

we obtain HAMILTON's principle for the electromechanic continuum

$$\delta\int_{t_1}^{t_2} L(u_i,\phi)\,\mathrm{d}t + \int_{t_1}^{t_2}\delta W(u_i,\phi)\,\mathrm{d}t = 0, \tag{2.18}$$

taking into account electrical and mechanical quantities. This principle states, that changes of theses quantities in a continuum are possible only in a manner

that satisfies (2.18). If it is now assumed, that displacement u_i and electric potential ϕ are independent state variables of a dielectric solid which are sufficient to determine the state of the solid uniquely[2)], then the possible states of the dielectric solid have to satisfy (2.18). There is a unique mapping of the state of the dielectric solid onto the electric enthalpy density H, and this function will determine the behavior of the dielectric solid, so (2.18) can be referred to as HAMILTON's principle for dielectric solids.

In some applications it might be preferable to choose displacement u_i and surface charge density $\sigma = -D_i n_i$ as independent quantities. As shown above, dependent and independent state variables in the energy expressions L and W can be interchanged by a LEGENDRE transformation, leading to a complementary form of HAMILTON's principle

$$\delta \int_{t_1}^{t_2} \widehat{L}(u_i, D_i)\,\mathrm{d}t + \int_{t_1}^{t_2} \delta\widehat{W}(u_i, D_i)\,\mathrm{d}t = 0 \tag{2.19}$$

where the transformed LAGRANGEian

$$\widehat{L} = \int_V (T - H - E_i D_i)\,\mathrm{d}V = \int_V (T - U)\,\mathrm{d}V \tag{2.20}$$

and a corresponding expression for the virtual work of external forces $\bar{f}_i$ and electric potential ϕ

$$\delta\widehat{W} = \delta W + \int_S \delta(\sigma\phi)\,\mathrm{d}S = \int_S (\bar{f}_i \delta u_i + \bar{\phi}\delta\sigma)\,\mathrm{d}S \tag{2.21}$$

have been introduced. The expressions (2.18) and (2.19) are equivalent, since

$$\begin{aligned} \delta \int_V E_k D_k\,\mathrm{d}V &= -\delta \int_V \phi_{,k} D_k\,\mathrm{d}V = -\delta \int_S \phi D_k n_k\,\mathrm{d}S + \delta \int_V \phi D_{k,k}\,\mathrm{d}V \\ &= \int_S \delta(\phi\sigma)\,\mathrm{d}S, \end{aligned} \tag{2.22}$$

taking into account, that the density of free charges in the dielectric solid is zero and therefore $D_{k,k} = 0$. It should be mentioned here, that the expression (2.19) is not a weak form of the problem (2.1)-(2.7), i.e. if the mathematical transformations applied in the course of the derivation of HAMILTON's principle in the form (2.18) are employed in reverse sequence, (2.19) does not lead to the equilibrium equations (2.1), (2.2) [WAS68]. Still, a variational principle in the form (2.19) can be useful to find approximate solutions, e.g. employing the RAYLEIGH-RITZ or GALERKIN method.

[2)] This assumption will generally be based on observation [REI96].

2.1.2 Constitutive equations

Piezoelectric solids exhibit a strong coupling between electrical and mechanical state variables. These state variables are interrelated via constitutive equations, which can be written in differential form

$$\begin{aligned} \mathrm{d}T_{ij} &= \frac{\partial T_{ij}}{\partial S_{kl}}\,\mathrm{d}S_{kl} + \frac{\partial T_{ij}}{\partial E_k}\,\mathrm{d}E_k, \\ \mathrm{d}D_i &= \frac{\partial D_i}{\partial S_{jk}}\,\mathrm{d}S_{jk} + \frac{\partial D_i}{\partial E_j}\,\mathrm{d}E_j, \end{aligned} \tag{2.23}$$

for strain and electric field as independent quantities, if all state changes are reversible [Rei96]. This implies the material is lossless, i.e. elastic and free of dielectric or piezoelectric losses. As a consequence of (2.23), there exists a potential U for the material, which can be represented in differential form by (2.11). The total differential of the electric enthalpy density H in the general form

$$\mathrm{d}H = \frac{\partial H}{\partial S_{ij}}\,\mathrm{d}S_{ij} + \frac{\partial H}{\partial E_i}\,\mathrm{d}E_i, \tag{2.24}$$

compared with (2.13) leads to

$$T_{ij} = \frac{\partial H}{\partial S_{ij}}, \qquad D_i = -\frac{\partial H}{\partial E_i}, \tag{2.25}$$

and the equations (2.23) become

$$\begin{aligned} \mathrm{d}T_{ij} &= \frac{\partial^2 H}{\partial S_{ij}\partial S_{kl}}\,\mathrm{d}S_{kl} + \frac{\partial^2 H}{\partial S_{ij}\partial E_k}\,\mathrm{d}E_k, \\ \mathrm{d}D_i &= -\frac{\partial^2 H}{\partial E_i\partial S_{jk}}\,\mathrm{d}S_{jk} - \frac{\partial^2 H}{\partial E_i\partial E_j}\,\mathrm{d}E_j. \end{aligned} \tag{2.26}$$

For the case of linear material behavior, the partial derivatives in (2.26) reduce to constants and the constitutive equations

$$\begin{aligned} T_{ij} &= c^E_{ijkl}S_{kl} - e_{kij}E_k, \\ D_i &= e_{ikl}S_{kl} + \varepsilon^S_{ik}E_k, \end{aligned} \tag{2.27}$$

are obtained for E_i and S_{ij} as independent variables. The superscripts E and S indicate that the corresponding constants have to be determined under constant electric field or strain conditions, respectively. Linear constitutive equations for

piezoelectric crystals were first given by VOIGT [VOI28]. From (2.26) and (2.27) it is obvious, that in the linear case the electric enthalpy density reads

$$H = \frac{1}{2} S_{ij} c^E_{ijkl} S_{kl} - E_i e_{ijk} S_{jk} - \frac{1}{2} E_i \varepsilon^S_{ij} E_j \tag{2.28}$$

and the internal energy density

$$U = H + E_i D_i = \frac{1}{2} S_{ij} c^E_{ijkl} S_{kl} + \frac{1}{2} E_i \varepsilon^S_{ij} E_j \tag{2.29}$$

is free of any terms involving coupling of electrical and mechanical quantities. If U is expressed in terms of E_i and T_{ij}

$$U = \frac{1}{2} T_{ij} s^E_{ijkl} T_{kl} + E_i d_{ijk} T_{jk} + \frac{1}{2} E_i \varepsilon^T_{ij} E_j, \tag{2.30}$$

coupling terms do occur. As in (2.26), linear constitutive equations can be obtained from the above expression in the form

$$\begin{aligned} S_{ij} &= s^E_{ijkl} T_{kl} + d_{kij} E_k, \\ D_i &= d_{ikl} S_{kl} + \varepsilon^T_{ik} E_k. \end{aligned} \tag{2.31}$$

In turn, for this set of constitutive equations, the corresponding expression for the electric enthalpy density

$$H = U - E_i D_i = \frac{1}{2} T_{ij} s^E_{ijkl} T_{kl} - \frac{1}{2} E_i \varepsilon^T_{ij} E_j \tag{2.32}$$

is free of coupling terms. The expressions (2.29) and (2.32) could mislead to the conclusion that upon their substitution in this form into the respective variational principles (2.18) and (2.19), the interaction between electrical and mechanical quantities would disappear. Whereas the change of the internal energy density δU and the electric enthalpy δH can apparently be derived from the corresponding potential functions U and H, this is generally not the case for the expressions $\delta\widehat{W}$ and δW. These represent the virtual work, which is performed on the dielectric solid under a virtual change of the independent state variables. The prescribed force $\bar{f}_i$, potential $\bar{\phi}$ and charge $\bar{\sigma}$ will generally be non-conservative i.e. arbitrary functions of time and they will not be related to the respective variations δu_i, $\delta\sigma$ and $\delta\phi$ by a potential function. Consequently, in the variational principles (2.19) and (2.18) the variations have to be carried out in the quantities given in the expressions for the virtual work and (2.29), (2.32) are then not suitable for substitution into these principles.

2.1.3 Electrical boundary conditions

In almost all of the technical applications of piezoelectric material, electrical boundary conditions will be prescribed on distinct electroded surfaces. On each of these surfaces, the potential ϕ will be constant over the area occupied by the electrode. Let the surface of the piezoelectric body be covered by N electrodes S_m , $(m = 1...N)$, of which k are subject to prescribed potential and the potential on these electrodes be denoted by $\bar{\phi}_m$, $(m = 1...k)$ for the prescribed case, and ϕ_m, $(m = k+1...N)$ for the free electrodes. On the k electrodes with prescribed potential $\bar{\phi}_m$, no variation $\delta\phi$ is admitted. For the remaining $N - k$ electrodes with free potential, the variation $\delta\phi$ in the surface integral

$$\int_{S_\sigma} (D_i n_i + \bar{\sigma})\delta\phi \, \mathrm{d}S = \sum_{m=k+1}^{N} \int_{S_m} (D_i n_i + \bar{\sigma})\delta\phi_m \, \mathrm{d}S \tag{2.33}$$

of expression (2.8) is not unconstrained, but has to be constant over the surface S_m, such that

$$\sum_{m=k+1}^{N} \int_{S_m} (D_i n_i + \bar{\sigma})\delta\phi_m \, \mathrm{d}S = \sum_{m=k+1}^{N} \delta\phi_m \left[\int_{S_m} D_i n_i \, \mathrm{d}S + \int_{S_m} \bar{\sigma} \, \mathrm{d}S \right] \tag{2.34}$$

and if we write for the total charge Q_m of each free electrode S_m

$$\int_{S_m} \bar{\sigma} \, \mathrm{d}S = Q_m; \qquad (m = k + 1...N), \tag{2.35}$$

the boundary condition (2.6) is replaced by an integral form

$$\int_{S_m} D_i n_i \, \mathrm{d}S + Q_m = 0; \qquad (m = k + 1...N), \tag{2.36}$$

which determines the unknown potential ϕ_m on the $N - k$ free electrodes. On the unelectroded part of the surface, the surface charge density is assumed to be equal to zero. Consequently, the partition S_σ of the total surface S of the piezoelectric body consists of free electrodes and the unelectroded part, whereas the remaining k electrodes represent S_ϕ. Internal electrodes will not be considered here.

2.1.4 Engineering notation

In the majority of the publications treating the computation of piezoelectric problems, a compressed matrix notation, often referred to as *'engineering notation'* is used. Making use of symmetry properties of the elastic and piezoelectric

tensors, the number of indices in the constitutive equations is reduced according to the following scheme [IEE88]:

ij or kl		p or q
11	$\rightarrow$	1
22	$\rightarrow$	2
33	$\rightarrow$	3
23 or 32	$\rightarrow$	4
31 or 13	$\rightarrow$	5
12 or 21	$\rightarrow$	6

Now, the constitutive equations (2.27) can be written in matrix form

$$\begin{aligned} T_p &= c_{pq}^E S_q - e_{kp} E_k, \\ D_i &= e_{iq} S_q + \varepsilon_{ik}^S E_k, \end{aligned} \tag{2.37}$$

where for the stress tensor

$$T_{ij} \rightarrow T_p, \tag{2.38}$$

the coefficients simply are rearranged in a one dimensional array. For the strain tensor, the transformation

$$\begin{aligned} S_{ij} &\rightarrow S_p, \quad \text{for} \quad i = j, \quad p = 1, 2, 3 \\ 2S_{ij} &\rightarrow S_p, \quad \text{for} \quad i \neq j, \quad p = 4, 5, 6 \end{aligned} \tag{2.39}$$

is employed, leading to analogous expressions for the internal energy density

$$\mathrm{d}U = T_{ij}\,\mathrm{d}S_{ij} + E_k\,\mathrm{d}D_k \quad \rightarrow \quad \mathrm{d}U = T_p\,\mathrm{d}S_p + E_k\,\mathrm{d}D_k \tag{2.40}$$

in the two systems [HN69]. Depending on the choice of the set of constitutive equations, some of the respective piezoelectric and elastic matrices have to be adapted accordingly, while others simply undergo the index reduction indicated above [IEE88].

2.2 Piezoceramic Solids

The interaction between mechanical and electrical field quantities in piezoelectric crystals is due to the lack of a center of symmetry in the charge distribution of

the crystal unit cell. Therefore, piezoelectric crystals are inherently anisotropic in their material properties [JS93]. What we consider a piezoceramic solid is initially a composition of a large number of randomly oriented piezoelectric crystals and isotropic on the macroscopic scale. Exposition to strong electric fields leads to partial reorientation of the crystal axes and the material is then polarized into a preferred direction [JCJ71]. As a consequence, polarized piezoceramic material exhibits planar isotropic behavior and the number of independent parameters, that constitute the linear material properties on the macroscopic scale, is significantly reduced compared to the most general case for piezoelectric crystals. Commonly, the axis of polarization is assumed to be the z- or 3-axis. The choice of the set of independent variables depends on the electrical and mechanical boundary conditions. For the models considered in this work, only one of the stress components is non-vanishing and constitutive equations of the form

$$\begin{aligned}
S_1 &= s_{11}^E T_1 + s_{12}^E T_2 + s_{13}^E T_3 + d_{31} E_3, \\
S_2 &= s_{12}^E T_1 + s_{11}^E T_2 + s_{13}^E T_3 + d_{31} E_3, \\
S_3 &= s_{13}^E T_1 + s_{13}^E T_2 + s_{33}^E T_3 + d_{33} E_3, \\
S_4 &= s_{44}^E T_4 + d_{15} E_2, \\
S_5 &= s_{44}^E T_5 + d_{15} E_1, \\
S_6 &= 2(s_{11}^E - s_{12}^E) T_6, \\
D_1 &= \varepsilon_{11}^T E_1 + d_{15} T_5, \\
D_2 &= \varepsilon_{11}^T E_2 + d_{15} T_4, \\
D_3 &= \varepsilon_{33}^T E_3 + d_{31}(T_1 + T_2) + d_{33} T_3,
\end{aligned} \tag{2.41}$$

are convenient to use. Of course, there are three other possible sets of linear constitutive equations for piezoceramic solids with (T_i, D_j), (S_i, D_j) or (S_i, E_j) as independent quantities [BCJ].

2.3 The Electromechanical Coupling Factor

The Electromechanical Coupling Factor k of a piezoelectric crystal was first introduced by Mason as *"the square root of the ratio of the energy stored in mechanical form, for a given type of displacement, to the total input electrical energy obtained from the input battery"*. Despite of the generality of this definition, the expression for the Electromechanical Coupling Factor (EMCF) in [Mas50] is merely a *material* coupling factor, which can be obtained from the

above definition under the assumption of homogeneous deformation of the piezoelectric solid [3)]. The analysis of equivalent circuits gave rise to the establishment of a relation between resonance and antiresonance frequencies of free vibrating piezoelectric transducers and the EMCF. This relation is often referred to as the *dynamic* [BCJ] or *effective* [HUN54] EMCF for vibrating transducers and will be discussed in section 2.3.2. Widely used is the definition for the EMCF given by the IEEE [IEE88], based on a quasistatic deformation cycle rather than energy expressions for a particular electroelastic state as it was the case in earlier definitions by the IRE [IRE58]. These definitions will be considered in section 2.3.1. To clarify some of the terminology used, in particular the terms *effective* and *material* coupling factor, the definition of the EMCF used in this work is introduced first.

The amount of energy which is converted by a thermodynamic system from one form into another depends on the path, which the state variables take in state space. So naturally, information about just one particular state cannot be sufficient to judge a system's ability to transform energy. To compare this ability for different paths and systems, a very intuitive restriction is to require the paths to be closed loops, so the energy conversion process can be carried out repeatedly and the system reaches its initial state after each cycle. A very well known closed-loop energy conversion process in thermodynamics is the CARNOT cycle, which was developed to investigate the efficiency of machines operating in cycles [REI96]. For piezoelectric transducers, feasible cycles in state space will be determined by HAMILTON's principle (2.18) and a corresponding electric enthalpy density, e.g. (2.28).

The EMCF used in this work is based on a quasi-static cycle of deformation and was introduced by ULITKO [ULI77]. It is defined according to

$$k^2 = \frac{U_{\text{conv}}}{U_{\text{oc}}} = \frac{U_{\text{oc}} - U_{\text{sc}}}{U_{\text{oc}}}, \tag{2.42}$$

as the square root of the ratio of the convertible to the total internal energy of the structure. Indices (oc) and (sc) refer to open circuited and short circuited electrodes, respectively. The convertible energy U_{conv} is the difference of the energy for open circuited electrodes U_{oc} and short circuited electrodes U_{sc} for a given strain field S_i. These energies will in general be represented by a volume integral. For linear constitutive relations, the energy U for a piezoceramic solid in the general form is represented by

$$U = \frac{1}{2} \int_V \left[T_i S_i + D_k E_k \right] \, \mathrm{d}V, \tag{2.43}$$

[3)] Also, a particularly simple geometry and electrode configuration is required.

and an explicit expression is obtained after substitution of the dependent pair of state variables by the independent pair via a set of constitutive equations e.g. of the form (2.27) leading to

$$\begin{aligned} U &= \frac{1}{2}\int_V \Big[c_{11}^E (S_1^2 + S_2^2) + c_{33}^E S_3^2 + \frac{1}{2}(c_{11}^E - c_{12}^E) S_6^2 + 2c_{12}^E S_1 S_2 \qquad (2.44) \\ &+ 2c_{13}^E (S_1 + S_2) S_3 + c_{44}^E (S_4^2 + S_5^2) + \varepsilon_{11}^S (E_1^2 + E_2^2) + \varepsilon_{33}^S E_3^2 \Big] \, \mathrm{d}V, \end{aligned}$$

where $2c_{66}^E = c_{11}^E - c_{12}^E$, for symmetry reasons. Expression (2.44) is convenient to compute the EMCF according to (2.42), as for a given strain distribution S_i, only the E_k depend on electrical boundary conditions. Still, depending on the problem, other choices might be preferred.

The EMCF is a measure for the relative amount of energy that can be converted from the mechanical to the electrical ports of the system and vice versa, in a quasistatic deformation cycle. To illustrate the definition (2.42), an example for the calculation of a *material* coupling factor, the longitudinal coupling factor k_{33}^{l} [IEE88], will be given.

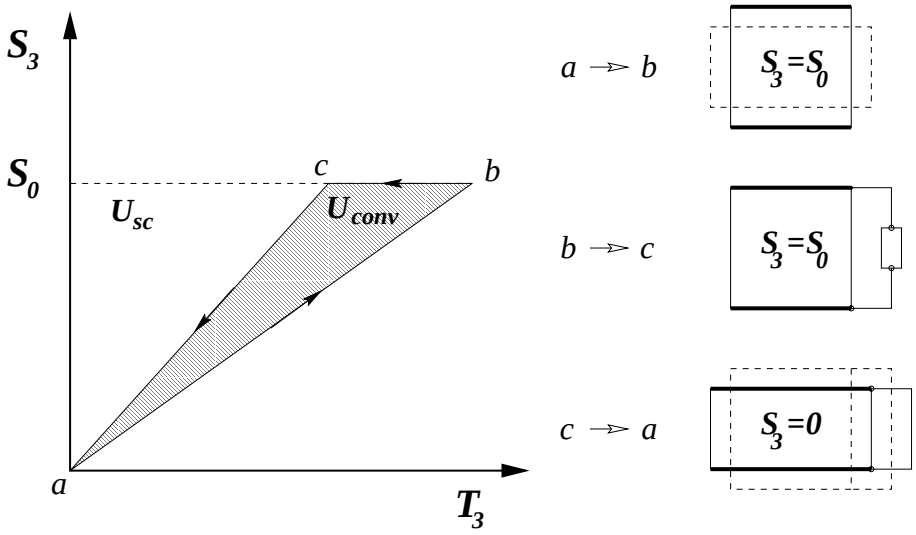

Figure 2.1: quasistatic deformation cycle

A piezoelectric rod, initially stress free with electroded top and bottom surfaces, which are initially charge free, is subjected to a prescribed **homogeneous** strain field $S_3 = S_0$ while the electrodes are open-circuited (free) and the rod is free to cross expand, i.e. $T_1, T_2 = 0$ (fig. 2.1). From the constitutive equations

(2.41), the stress T_3 and electric field E_3 corresponding to state b are

$$T_3 = S_0 \frac{\varepsilon_{33}^T}{\varepsilon_{33}^T s_{33}^E - d_{33}^2}, \qquad E_3 = S_0 \frac{d_{33}}{d_{33}^2 - \varepsilon_{33}^T s_{33}^E}, \tag{2.45}$$

taking into account, that $D_3 = 0$ at the electroded surfaces for charge free electrodes and such for the entire volume[4)] of the piezoelectric rod. The energy U_{oc} is computed as

$$U_{\mathrm{oc}} = \frac{1}{2} V S_0^2 \frac{\varepsilon_{33}^T}{\varepsilon_{33}^T s_{33}^E - d_{33}^2}, \tag{2.46}$$

E_3 and T_3 being the only non-vanishing variables in (2.43). V is the volume of the rod.

The electrodes are then connected to an ideal electric load[5)], under **constant strain** S_0 and state c is reached. The work done on the ideal electric load is the convertible energy of the system. Now, we have equal potential on the electrodes and $E_3 = 0$. For short-circuited electrodes, the stress T_3 under given strain S_0 becomes

$$T_3 = \frac{S_0}{s_{33}^E}, \tag{2.47}$$

and the energy is

$$U_{\mathrm{sc}} = \frac{1}{2} V S_0^2 \frac{1}{s_{33}^E}, \tag{2.48}$$

where only T_3 and S_3=S_0 contribute to the energy expression (2.43). To complete the cycle, the strain field is removed, while the electrodes remain short-circuited and the rod is back in its initial state a. The coupling factor (2.42) for this deformation cycle becomes

$$(k_{33}^1)^2 = \frac{\frac{\varepsilon_{33}^T}{\varepsilon_{33}^T s_{33}^E - d_{33}^2} - \frac{1}{s_{33}^E}}{\frac{\varepsilon_{33}^T}{\varepsilon_{33}^T s_{33}^E - d_{33}^2}} = \frac{d_{33}^2}{\varepsilon_{33}^T s_{33}^E}, \tag{2.49}$$

and the particularly simple form of this expression is a result of the homogeneous one-dimensional deformation S_0 and the simple geometry of the piezoelectric rod. It should be noted here, that the result of this computation depends on the condition $T_1, T_2 = 0$ for longitudinal expansion of the rod. The shaded area

[4)] According to (2.2), the electric displacement is divergence free, i.e. $D_{3,3} = 0$ inside the piezoelectric body, where the density of free charges ρ_{f} is zero. So if D_3 is continuous and zero on the surface it has to be zero in the entire volume.

[5)] This could be an ordinary resistor leading to an exponential decay of the potential difference on the electrodes. It is ideal in the sense that zero potential difference is reached in finite time and the procedure still can be considered quasistatic.

in the T_3, S_3 diagram (fig. 2.1) represents the convertible energy U_{conv} of the quasistatic deformation cycle.

k_{33}^{l} is called a *material* coupling factor because the expression (2.49) contains only constitutive parameters and therefore defines a material property. If the one dimensional strain field S_0 was not homogeneous, the expression (2.49) would rather be a fraction of integral terms of the form (2.43), and the resulting *effective* EMCF for inhomogeneous longitudinal deformation would always be smaller than k_{33}^{l}. Also, the electrode geometry has an impact on the *effective* EMCF. So in the general case of inhomogeneous deformation, the resulting coupling factor calculated according to definition (2.42) would always be the *effective* coupling factor. Only in the case of homogeneous fields, the resulting expression reduces to a *material* coupling factor. For the terminology used in this work, the term *effective* will be omitted, and the EMCF shall be understood as related to a particular mode of deformation according to definition (2.42).

The definition (2.42) is convenient, because it relates to an arbitrary mode of deformation of an electroded piezoelectric body, whereas material coupling factors simply represent a set of constitutive parameters. Consequently, the EMCF in this form can be used as a design criterion in actuator applications, where the performance of the actuator as an energy transmitter does not only depend on its material properties, but also on geometry, electrode shape and deformation.

Clearly, in this definition no losses or dynamic effects are taken into account.

2.3.1 IEEE/IRE standards definitions

An early definition given in the *IRE Standard on Piezoelectricity* of 1958 [IRE58], which is still occasionally found in the literature [LP91], [Ler90], is based on energy expressions containing coupling terms similar to (2.30) which constitute linear interaction between state variables. Accordingly, the EMCF is defined as

$$k_{\mathrm{IRE}}^2 = \frac{{U_{\mathrm{m}}}^2}{U_{\mathrm{e}} U_{\mathrm{d}}}, \tag{2.50}$$

where the so-called mutual, elastic and dielectric energies are given by

$$U_{\mathrm{m}} = E_i d_{ijk} T_{jk}, \qquad U_{\mathrm{e}} = T_{ij} s_{ijkl}^E T_{kl}, \qquad U_{\mathrm{d}} = E_i \varepsilon_{ij}^T E_j, \tag{2.51}$$

respectively, with (2.30) as the energy expression. In this form, the EMCF can be calculated per volume element and in the general case of inhomogeneous field distributions, the EMCF for a given structure will be obtained by volume integration.

In the case of simple homogeneous fields, (2.50) delivers the expected material coupling factors introduced above. However, the definition (2.50) suffers from at least one severe drawback. If the electroelastic state for a transducer can be represented by one-dimensional fields, e.g. T_1 and E_3, k_{IRE} reduces to a material coupling factor **independent** of the deformation mode. For the given example, with (2.30) as the energy function and T_1, E_3 as the independent variables, k_{IRE} becomes

$$\frac{{U_{\mathrm{m}}}^2}{U_{\mathrm{e}}U_{\mathrm{d}}} = \frac{(E_3 d_{31} T_1)^2}{T_1 s_{11}^E T_1 \, E_3 \varepsilon_{33}^T E_3} = \frac{d_{31}^2}{s_{11}^E \varepsilon_{33}^T} = k_{31}^2,$$

where k_{31} is the material coupling factor for longitudinal deformation of a thickness polarized piezoelectric rod [BCJ], which plays an important role in bending actuation applications.

The above definition (2.50) was abandoned, and replaced by a new definition in 1978 [IEE78] which is based on a quasi-static stress cycle. It remained unchanged since then and in the ANSI/IEEE standard of 1987 [IEE88], which is currently under revision, the calculation of the material EMCF k_{33}^{l} is described as follows (see fig. 2.2):

"The element is plated on faces perpendicular to x_3, the polar axis, and is short-circuited as a compressive stress $-T_3$ is applied. The element is free to cross expand, so that T_3 is the only nonzero stress component. From the figure it can be seen, that the total stored energy per unit volume at maximum compression is $W_1 + W_2$. Prior to removal of the compressive stress, the element is open-circuited. It is then connected to an ideal electric load to complete the cycle. As work is done on the electric load, the strain returns to its initial state. For the idealized cycle illustrated, the work W_1 done on the electric load and the part of the energy unavailable to the electric load W_2 are related to the coupling factor k_{33}^l as follows:"

$$(k_{33}^{\mathrm{l}})^2 = \frac{W_1}{W_1 + W_2} = \frac{s_{33}^E - s_{33}^D}{s_{33}^E} = \frac{d_{33}^2}{s_{33}^E \varepsilon_{33}^T} \tag{2.52}$$

This definition gives the same result for k_{33}^{l} as (2.42) and could be extended to nonhomogeneous fields with no extra effort. For nonlinear material properties,

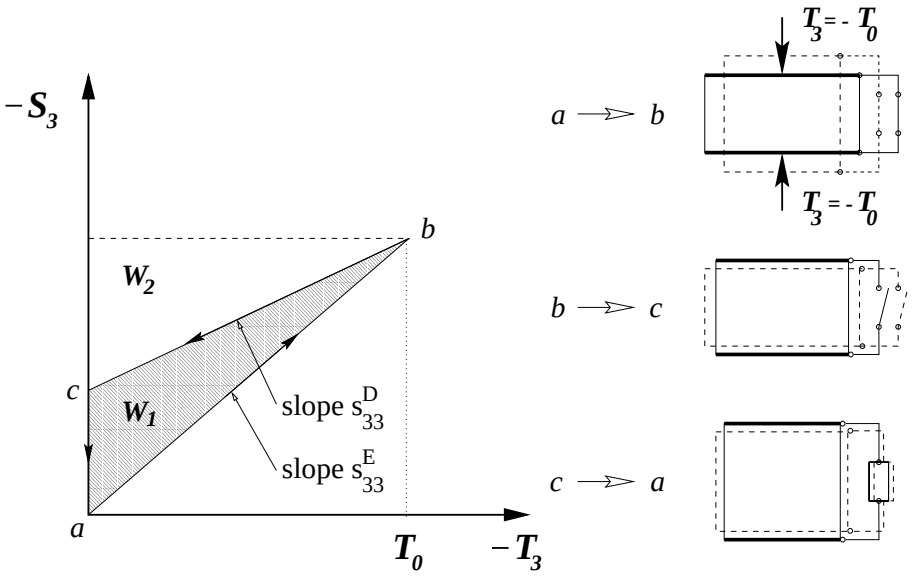

Figure 2.2: quasistatic stress cycle

the EMCF can be computed for a prescribed stress cycle [HPS+94] and the extension of the definition (2.42) to nonlinear constitutive relations would equally be possible. The evaluation of the energy expressions will then generally require numerical integration. However, the current standard [IEE88] limits the application to linear material properties, homogeneous fields and material coupling factors.

2.3.2 Dynamic/Effective EMCF

The definition (2.42) of the electromechanical coupling factor given above, refers to a particular prescribed mode of deformation of the actuator. In transducer applications, the mode and amplitude of vibration will depend on the frequency of excitation and so will the performance of the actuator. On the other hand, the frequency characteristics of an actuator can be used to estimate its electromechanical coupling ability [BCJ]. For any conservative electromechanical system vibrating freely in an eigenmode

$$u_i(x_k,t) = \hat{u}_i(x_k)\cos\Omega t, \tag{2.53}$$

$$\phi(x_k,t) = \hat{\phi}(x_k)\cos\Omega t, \tag{2.54}$$

the maximum kinetic energy

$$T_{\max} = \frac{1}{2}\Omega^2 \int_V \rho\, \hat{u}_i \hat{u}_i \,\mathrm{d}V \tag{2.55}$$

equals the maximum internal energy

$$U_{\max} = \frac{1}{2} \int_V (\hat{T}_i \hat{S}_i + \hat{D}_k \hat{E}_k) \,\mathrm{d}V \tag{2.56}$$

computed for the mode of vibration $[\hat{u}_i, \hat{\phi}]$. If the displacement field $\hat{u}_i\,(x_k)$ is given, the electric potential field $\hat{\phi}\,(x_k)$ and also the internal energy $U_{\max}$ of the system depend on the electrical boundary conditions. In particular, for open or short-circuited electrodes the internal energies would be different for the same displacement field.

In the case of forced vibration of a conservative system excited by a piezoelectric actuator, resonance occurs when the frequency of excitation matches the resonance frequency f_r, which is the eigenfrequency of the same system with the electrodes of the actuator short-circuited. In this case, the electrical impedance of the system is zero. The eigenfrequencies of the system with free electrodes are the so-called antiresonance frequencies f_a. Being excited at these frequencies, the system vibrates in the corresponding antiresonance modes and the electric impedance of the system is infinite i.e. the amplitude of the electric current is zero.

Both, the resonance and the antiresonance mode are eigenmodes of the system, for short-circuited or open electrodes, respectively. Now, for the particular (hypothetical) case where the displacement fields of resonance and antiresonance are identical, the respective internal energies are computed for the same deformation but different electrical boundary conditions. Recalling the definition (2.42) and having in mind, that (2.55) and (2.56) are equal, it follows that

$$k_\mathrm{d}^2 = \frac{U_\mathrm{oc} - U_\mathrm{sc}}{U_\mathrm{oc}} = \frac{\Omega_\mathrm{a}^2 - \Omega_\mathrm{r}^2}{\Omega_\mathrm{a}^2} = \frac{f_\mathrm{a}^2 - f_\mathrm{r}^2}{f_\mathrm{a}^2} \tag{2.57}$$

for the case of **identical resonance and antiresonance modes** of deformation. This is actually the case for the ballooning vibration mode of a thin piezoelectric ring or spherical shell [BCJ], polarized in radial direction and fully electroded on the inside and outside.

The frequency relation (2.57) is also referred to as the *effective* or *dynamic* electromechanical coupling factor [Hun54], [BCJ] of a piezoelectric resonator.

Resonance and antiresonance frequencies f_r, f_a of a vibrating actuator can easily be obtained by impedance measurements. MASON computed material coupling factors for different piezoelectric materials from impedance measurements of longitudinally vibrating piezoelectric crystals [MAS50], but it was not his intention to classify the performance of different transducers regarding energy conversion. The relation (2.57) originated from equivalent circuit considerations. Representing a piezoelectric resonator by a simple equivalent circuit corresponds to a modal discretization in one degree of freedom. It is no surprise, that the relation (2.57) always holds for such an approximation, as resonance and antiresonance modes are then necessarily identical.

The relation (2.57) is useful to compute approximate values of the EMCF of an electroelastic system from impedance measurements which deliver the resonance and antiresonance frequencies. These approximate values correspond to those obtained from definition (2.42), if the prescribed strain field is the resonance mode of vibration. Generally, the accuracy of this approximation will be good if resonance and antiresonance modes are similar i.e. if the corresponding frequencies are close and consequently the values for k_d are small. Dynamic effects are considered only in the sense that the underlying mode of deformation is the resonance mode. Still, the cycle (fig. 2.1) that the structure is assumed to undergo to determine the amount of energy converted, is a quasi-static hypothetical process and not representative for the behavior of a dynamic system.

Chapter 3

Optimal Design

A useful optimization criterion to be employed in the design process of piezoceramic actuators should give satisfying results for a variety of applications. On the other hand, it should be very general and straightforward to use, with as little as possible information required on the particular structure, the actuator is going to be attached to. One crucial aspect will be the bonding of the actuator to the structure, but information about e.g. the thickness of the bonding layer might be difficult, if not impossible, to obtain. Of course, the energy transfer into the structure will depend on its ability to emit energy itself, i.e. mechanical boundary conditions. Again, these might be hard to determine, even if the complete design of the structure is given. The structures under investigation here are slender beams, i.e. the ratio of the longitudinal to the transverse dimensions is large and they are assumed to deform according to the Bernoulli-Euler hypothesis. The optimization variable will be the thickness of the piezoelectric layer of the laminated beam. Under operating conditions, the performance of the actuator will depend on the deformation and generally this deformation will again depend on the thickness of the actuator. However, for analytical treatment of the problem, the influence of changing actuator thickness on the beam vibrations can only be considered for particularly simple geometries and boundary conditions.

Models of the bending actuation of piezoelectric patches on beams and plates have been presented by several authors [CR94]. Among them, the earliest so-called *Pin-Force* models for actuator pairs bonded symmetrically to both surfaces

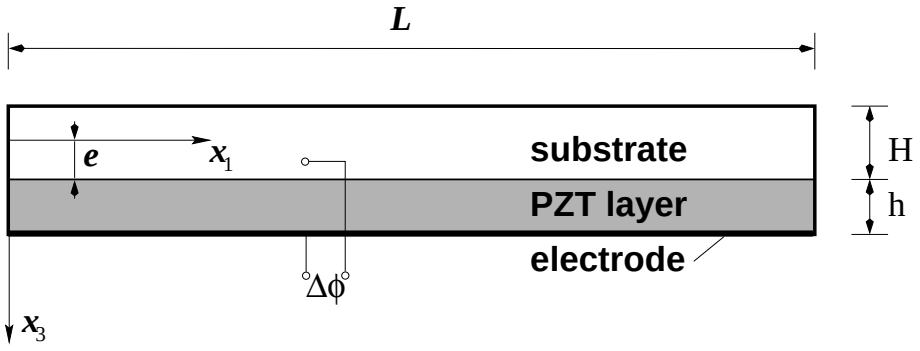

Figure 3.1: laminate beam structure

of a beam were introduced by Crawley, de Luis and Anderson [CdL87], [CA90]. Pin-Force models neglect the added bending stiffness and mass effects due to the actuator patches. They are not suitable for the modeling of thick piezoelectric layers on thin substrate beams [SBG95], [CR94]. Euler-Bernoulli models assume a linear strain distribution in the piezoelectric layer and include the added stiffness and mass of the actuator patches [BSW95]. For actuators bonded to one side only, longitudinal and flexural vibrations are generally coupled [SBG95]. An assumption common to all the models is that the electric field in the piezoelectric layer be independent of the thickness coordinate, which does not comply with Gauss's law (2.2). It will be shown that this simplification is unnecessary and the correct linear distribution of the electric field can be incorporated into the model without effort [GUS89].

3.1 The Laminate Beam

The portions of the beam to which actuators are bonded form a laminate, consisting of the piezoceramic layer, which is electroded on the outward face, and the substrate material (fig. 3.1). The substrate layer is assumed to be conductive and serves as the second electrode, such that a potential difference $\Delta\phi$ can be applied between the electrode and the substrate layer.

In compliance with the Bernoulli-Euler hypothesis, the cross sections of the laminate remain plane and perpendicular to the neutral axis, which is located

at a distance e to the interface layer and is inextensible, i.e. the laminate is assumed to undergo pure bending deformation. The longitudinal displacement u_1 in the laminate is then

$$u_1(x_1, x_3) = -x_3 w'(x_1), \tag{3.1}$$

and the longitudinal strain

$$S_1 = u_{1,1} = -x_3 w''(x_1) \tag{3.2}$$

follows from (2.10). The transverse stresses T_2, T_3 and shearing stresses T_4, T_5, T_6 are assumed to vanish as well as the shearing strains S_4, S_5, S_6. Of the electrical quantities, the only nonzero components are E_3, D_3, so we have 12 additional equations:

$$T_2, T_3, T_4, T_5, T_6, S_4, S_5, S_6, D_1, D_2, E_1, E_2 = 0. \tag{3.3}$$

Given these assumptions, the constitutive equations (2.41) reduce to

$$S_1 = s_{11}^E T_1 + d_{31} E_3, \tag{3.4}$$

$$D_3 = \varepsilon_{33}^T E_3 + d_{31} T_1, \tag{3.5}$$

where the expressions for longitudinal strains S_2, S_3 have been omitted as these do not contribute to the internal energy U (2.43) and therefore do not provide any essential information. Substitution of (3.2) and (3.4) into (3.5) yields

$$D_3 = (1 - k_{31}^2)\varepsilon_{33}^T E_3 - \frac{d_{31}}{s_{11}^E} x_3 w''(x_1) \tag{3.6}$$

for the electric displacement. The expression (3.6) has been simplified by the introduction of

$$k_{31}^2 = \frac{d_{31}^2}{s_{11}^E \varepsilon_{33}^T}, \tag{3.7}$$

which would be the EMCF of the piezoelectric layer (fig. 3.1) for uniform longitudinal strain.[1)] From (2.2) it is seen, that the electric displacement is constant over the thickness coordinate ($D_{3,3} = 0$) which in connection with (3.6) leads to

$$(1 - k_{31}^2)\varepsilon_{33}^T E_{3,3} = \frac{d_{31}}{s_{11}^E} w''(x_1), \tag{3.8}$$

[1)] This is true for $T_2, T_3 = 0$. A uniform (homogeneous) longitudinal strain field corresponds to a uniform longitudinal extension, which does not comply with the strain field (3.2).

and the conclusion, that the electric field E_3 is a linear function of the thickness coordinate x_3. Consequently, the potential ϕ which is related to the electric field by (2.3) must be of the form

$$\phi(x_1, x_3) = \phi_0(x_1) + \phi_1(x_1)x_3 + \phi_2(x_1)x_3^2, \tag{3.9}$$

so that

$$E_3 = -\frac{\partial}{\partial x_3}\left[\phi(x_1, x_3)\right] = -\phi_1(x_1) - 2\phi_2(x_1)x_3 \tag{3.10}$$

where the unknown functions $\phi_1(x_1), \phi_2(x_1)$ have to be determined from (2.7) and (3.8). The latter of these expressions leads to

$$\phi_2(x_1) = -\frac{1}{2}\frac{k_{31}^2}{d_{31}(1-k_{31}^2)}w''(x_1). \tag{3.11}$$

An electric potential can only be defined relative to a reference and not as an absolute value. Therefore, only the potential difference between the electrode and the substrate

$$\phi(x_1, e+h) - \phi(x_1, e) = \Delta\phi \tag{3.12}$$

can be prescribed for the laminate (fig. 3.1). ϕ_1 is now obtained by substitution of (3.9) together with (3.11) into (3.12) and the resulting electric field

$$E_3 = \frac{\Delta\phi}{h} - \frac{1}{d_{31}(1-k_{31}^2)}\left[\left(e+\frac{h}{2}\right) - x_3\right]w''(x_1) \tag{3.13}$$

is uniquely determined by the potential difference $\Delta\phi$ and the curvature $w''(x_1)$ of the laminate. Given the electric field, the longitudinal stress

$$T_1 = \frac{1}{s_{11}^E}\left[k_{31}^2\left(e+\frac{h}{2}\right) - x_3\right]w''(x_1) - \frac{d_{31}}{s_{11}^E}\frac{\Delta\phi}{h} \tag{3.14}$$

follows from (3.4). The internal energy expression (2.43) with (3.3) boils down to

$$U = \frac{1}{2}\int_V \left[s_{11}^E T_1^2 + \varepsilon_{33}^T E_3^2 + 2d_{31}E_3T_1\right]\,\mathrm{d}V, \tag{3.15}$$

where E_3, T_1 are given by (3.13),(3.14) respectively. For given displacement $w(x_1)$, (3.15) delivers the internal energy, depending on the potential difference $\Delta\phi$. For short circuited electrodes ($\Delta\phi = 0$),

$$U_{\mathrm{sc}} = \frac{1}{2}\frac{bh}{s_{11}^E}\left[\left(e+\frac{h}{2}\right)^2 + \frac{1}{(1-k_{31}^2)}\frac{h^2}{12}\right]\int_0^L \left[w''(x_1)\right]^2\,\mathrm{d}x_1 \tag{3.16}$$

is obtained after integration over the volume V of the piezoelectric layer. To complete the expression (2.42), still the internal energy must be computed for

open circuited electrodes. The unknown potential difference between the electrode and the substrate follows then from the integral boundary condition (2.36). The electric displacement D_3 yet has not been expressed as a function of $\Delta\phi$ and displacement $w(x_1)$. Substitution of (3.13) into (3.6) yields

$$D_3 = (1 - k_{31}^2)\varepsilon_{33}^T \frac{\Delta\phi}{h} + \frac{d_{31}}{s_{11}^E}\left(e + \frac{h}{2}\right) w''(x_1), \tag{3.17}$$

and presuming, that the electrode and substrate are initially charge free, (2.36) turns into

$$\int_0^L D_3 \, \mathrm{d}x_1 = 0, \tag{3.18}$$

which would have to be evaluated at the boundary $x_3 = e$ or $x_3 = e+h$ if D_3 was depending on the thickness coordinate. With the resulting potential difference

$$\Delta\phi_{\mathrm{oc}} = \frac{k_{31}^2}{d_{31}(1 - k_{31}^2)} \frac{h}{L}\left(e + \frac{h}{2}\right) w'(x_1)|_0^L, \tag{3.19}$$

the internal energy U_{oc} corresponding to state b (fig. 3.1) is found. Using

$$U_{\mathrm{oc}} = U_{\mathrm{sc}} + U_{\mathrm{conv}}, \tag{3.20}$$

a relatively compact expression for the convertible energy

$$U_{\mathrm{conv}} = \frac{1}{2}\frac{bh}{s_{11}^E}\frac{k_{31}^2}{(1 - k_{31}^2)}\left(e + \frac{h}{2}\right)^2 \frac{1}{L}\left[w'(x_1)|_0^L\right]^2 \tag{3.21}$$

is obtained. The expression for U_{oc} is then simply the sum of (3.16) and (3.21).

3.2 Maximum EMCF

The definition (2.42) of the electromechanical coupling factor suggests, that only contributions of piezoelectric material to the internal energy are to be accounted for. However, it is by no means restricted to piezoelectric material. The laminate structure under investigation is composed of the piezoelectric layer and the non piezoelectric substrate layer. Given (3.3), the longitudinal stress in the substrate becomes

$$T_1^{(\mathrm{s})} = E_{\mathrm{s}} S_1, \tag{3.22}$$

where E_s is YOUNG's modulus of the substrate material. The energy contribution of the substrate layer

$$U_\mathrm{s} = \frac{1}{2}\int_{V_\mathrm{s}} S_1 T_1^{(\mathrm{s})}\,\mathrm{d}V_\mathrm{s} = \frac{1}{2} bHE_\mathrm{s}\left(e-\frac{H}{2}\right)^2 \int_0^L w''(x_1)^2\,\mathrm{d}x_1 \tag{3.23}$$

is again obtained by integration over the corresponding volume V_s of the substrate and U_s is obviously independent of electrical boundary conditions.

So far, all of the energy expressions (3.16), (3.21) and (3.23) still depend on the distance e of the laminate's neutral axis to the interface layer. Demanding that the normal force, i.e. the integral of the longitudinal stress over the cross-sectional area, vanishes for the given pure bending deformation, the neutral axis is determined from

$$\int_{e-H}^{e} T_1^{(\mathrm{s})}\,\mathrm{d}x_3 + \int_e^{e+h} T_1\,\mathrm{d}x_3 = 0, \tag{3.24}$$

which, in connection with (3.22) and (3.14) results in

$$e = \frac{H}{2}\frac{E_\mathrm{s}s_{11}^E - \frac{h^2}{H^2}}{E_\mathrm{s}s_{11}^E + \frac{h}{H}} \tag{3.25}$$

for the location of the origin of the coordinate frame. Being not influenced by electrical boundary conditions, (3.23) will clearly not contribute to the structure's convertible energy, but rather to U_oc in the definition (2.42). The EMCF, augmented by the contribution U_s of non piezoelectric material is then given by

$$k^2 = \frac{U_\mathrm{conv}}{U_\mathrm{sc} + U_\mathrm{conv} + U_\mathrm{s}}, \tag{3.26}$$

a rather bulky expression, which is a functional of the prescribed deformation $w(x_1)$. For a given mode of deformation, (3.26) becomes an explicit function of the thickness ratio $\gamma = \frac{h}{H}$ of the layers only. However, (3.26) is an expression of the form

$$k^2(w,\gamma) = \frac{f_\mathrm{conv}(\gamma)}{F\left[w(x_1)\right]\left[f_\mathrm{sc}(\gamma) + f_\mathrm{s}(\gamma)\right] + f_\mathrm{conv}(\gamma)}, \tag{3.27}$$

where the only term depending on the prescribed deformation is the functional

$$F\left[w(x_1)\right] = \frac{1}{\left[w'(x_1)|_0^L\right]^2}\int_0^L \left[w''(x_1)\right]^2\,\mathrm{d}x_1. \tag{3.28}$$

Now, assuming that the mode of deformation $w(x_1)$ and the thickness ratio γ are not interrelated[2)], the derivative of (3.27) taken with respect to γ

$$\frac{\mathrm{d}}{\mathrm{d}\gamma}\left[k^2(w,\gamma)\right] = F\left[w(x_1)\right]\frac{f'_{\mathrm{conv}}(\gamma)\left[f_{\mathrm{s}}(\gamma)+f_{\mathrm{sc}}(\gamma)\right]-f_{\mathrm{conv}}(\gamma)\left[f'_{\mathrm{s}}(\gamma)+f'_{\mathrm{sc}}(\gamma)\right]}{\left\{F\left[w(x_1)\right]\left[f_{\mathrm{sc}}(\gamma)+f_{\mathrm{s}}(\gamma)\right]+f_{\mathrm{conv}}(\gamma)\right\}^2} \tag{3.29}$$

shows, that extremal values of the EMCF, i.e. values of k^2 for which

$$\frac{\mathrm{d}}{\mathrm{d}\gamma}\left[k^2(w,\gamma)\right] = 0, \tag{3.30}$$

can be found for values of the thickness ratio γ, which satisfy the condition

$$f'_{\mathrm{conv}}(\gamma)\left[f_{\mathrm{s}}(\gamma)+f_{\mathrm{sc}}(\gamma)\right]-f_{\mathrm{conv}}(\gamma)\left[f'_{\mathrm{s}}(\gamma)+f'_{\mathrm{sc}}(\gamma)\right] = 0, \tag{3.31}$$

independently of the deformation $w(x_1)$ of the laminate. Following the above procedure, substituting the expressions (3.23), (3.21), (3.16) with (3.25) into (3.26) and taking the derivative with respect to γ, the condition (3.31) for extremal values can be written in the form

$$\mu^2(1+\gamma)(\gamma^2+2\gamma+\mu)(2\gamma^4+5\mu\gamma^3+3\mu\gamma^2-3\mu^2\gamma-\mu^2) = 0, \tag{3.32}$$

showing that only the ratio of the longitudinal stiffnesses of the layers $\mu = E_{\mathrm{s}}s^E_{11}$, and not piezoelectric or dielectric constants, determine the thickness ratio for maximum electromechanical coupling according to definition (2.42). Computational results for the EMCF depending on the thickness ratio are given in chapter four.

3.3 Maximum Dynamic EMCF

The optimal thickness for maximum EMCF based on definition (2.42) of the laminate beam was independent of the assumed deformation. For a vibrating electromechanical system, the changing actuator thickness will generally have an impact on the mode of vibration. For the particular case of a periodic laminate

[2)] Generally, the mode of vibration of a piezoelectric laminate will depend on the thickness ratio of the two layers. This dependence can only be modeled, if explicit solutions to the equations of motion are available. The EMCF is computed for a prescribed mode of deformation here, and a possible influence of the thickness ratio on this mode is neglected for the optimization.

beam (fig. 3.2), explicit solutions for the equations of motion can be found and the dynamic EMCF can be computed according to definition (2.57). The dashed lines mark the locations where periodic boundary conditions apply. The piezoelectric bottom layer is polarized in thickness direction with alternating orientation corresponding to the distinctly shaded areas. A harmonic voltage $\Delta\phi = U_0 \sin(\Omega t)$ is applied between the bottom electrode and the substrate layer.

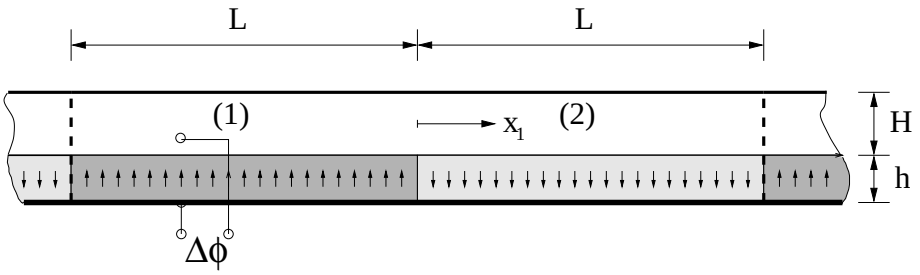

Figure 3.2: periodic laminate beam system

For the periodic laminate beam, given the assumptions (3.2), (3.3), the general form (2.12) of the electric enthalpy density reduces to

$$H = \frac{1}{2}(T_1 S_1 - D_3 E_3) \tag{3.33}$$

for linear constitutive relations (3.4),(3.5), which upon substitution of (3.2), (3.6), (3.13), (3.14) and integration over the thickness h of the layer leads to

$$\begin{aligned} H_\mathrm{p} &= \frac{1}{2}\frac{bh}{s_{11}^E}\int_0^L \left[\left(\frac{\Delta\phi}{h}\right)^2 + 2d_{31}\left(e+\frac{h}{2}\right)\frac{\Delta\phi}{h}w''(x_1)\right. \\ &+ \left.\left[\left(e+\frac{h}{2}\right)^2 + \frac{1}{1-k_{31}^2}\frac{h^2}{12}\right]\left[w''(x_1)\right]^2\right] \mathrm{d}x_1 \end{aligned} \tag{3.34}$$

for the electric enthalpy of the piezoelectric layer. For the substrate layer, the quantities E_3 and D_3 vanish, such that internal energy density U and electric enthalpy density H are equivalent here (2.12). Consequently, (3.23) represents the contribution of the substrate layer to the electric enthalpy of the laminate and with the corresponding LAGRANGEian (2.16), HAMILTON's principle for the laminate is written as

$$\int_{t_1}^{t_2}\left[\int_0^L \frac{1}{2}\rho bh\,\delta\dot{w}^2\,\mathrm{d}x_1 - \delta(H_p + U_s)\right]\mathrm{d}t + \int_{t_1}^{t_2}\int_S (\bar{\sigma}\delta\phi - \bar{f}\delta u_i)\,\mathrm{d}S\,\mathrm{d}t = 0, \tag{3.35}$$

and the displacement $w(x_1,t)$ is now time dependent. After partial integration, the expression

$$\int_0^L (Cw^{\mathrm{IV}} + \rho bh\ddot{w})\delta w \,\mathrm{d}x_1 - Cw'''\delta w|_0^L + [Cw'' + M_0]\,\delta w'|_0^L = 0 \tag{3.36}$$

is obtained, where the effective bending stiffness

$$C = \frac{bh}{s_{11}^E}\left[\left(e+\frac{h}{2}\right)^2 + \frac{1}{1-k_{31}^2}\frac{h^2}{12}\right] + bHE_{\mathrm{s}}\left[\left(e-\frac{H}{2}\right)^2 + \frac{H^2}{12}\right] \tag{3.37}$$

of the laminate and the actuation bending moment

$$M_0(t) = b\frac{d_{31}}{s_{11}^E}\left(e+\frac{h}{2}\right)\Delta\phi(t)$$

have been introduced.

For forced vibrations induced by the harmonic voltage $\Delta\phi(t) = U_0\sin(\Omega t)$, solutions are found in the form

$$w(x_1,t) = \frac{1}{2}\frac{M_0}{CK^2}\left[\frac{\cos K(x_1+\frac{L}{2})}{\cos K\frac{L}{2}} - \frac{\cosh K(x_1+\frac{L}{2})}{\cosh K\frac{L}{2}}\right] \tag{3.38}$$

where the wave number K is defined by the dispersion relation

$$K^4 = \Omega^2\frac{\rho b(h+H)}{C} \tag{3.39}$$

[Fre97], [WFHS97]. Resonant modes of vibration of the laminate are represented by wave numbers K which satisfy

$$\cos K\frac{L}{2} = 0,$$

and the corresponding resonance frequencies are then obtained from the dispersion relation (3.39).

The charge on the bottom electrode is determined by (2.36) and (3.17) leading to

$$Q_{\mathrm{s}}(t) = 2bL\left[\varepsilon_{33}^T\frac{\Delta\phi(t)}{h}(1-k_{31}^2) + \frac{d_{31}}{s_{11}^E}(e+\frac{h}{2})\left[w'(t)|_0^L - w'(t)|_{-L}^0\right]\frac{1}{2L}\right] \tag{3.40}$$

and the time derivative of this expression gives the current through the considered part of the periodic system. Upon substitution of the solution (3.38) into (3.40) and taking the time derivative, the condition for zero current

$$\tan\frac{KL}{2}+\tanh\frac{KL}{2}+KL\frac{Cs_{11}^{E}}{bh(e+\frac{h}{2})^2}\frac{(1-k_{31}^2)}{k_{31}^2}=0 \tag{3.41}$$

is obtained. Wave numbers that satisfy this expression have to be determined numerically. They represent the antiresonance modes of the laminate and the corresponding antiresonance frequencies $f_a=\Omega_a/2\pi$ result again from the dispersion relation (3.39). The dynamic EMCF

$$k_d^2=\frac{f_a^2-f_r^2}{f_a^2} \tag{3.42}$$

is numerically computed for the periodic system (fig. 3.2) for different thickness ratios H/h of the layers. Results are given in chapter four.

3.4 Maximum Power Factor

The EMCF is a measure for the fraction of the maximal work supplied to a electromechanical system, which is converted in a quasi-static deformation cycle. This cycle has hypothetical character and is convenient for computation, but dynamic load cycles will generally be different. The consideration of dynamic cycles in this work is restricted to steady state vibrations of linear electroelastic systems. Then, the load cycles are ellipses in the (T_i,S_i) and (E_k,D_k) state planes and it is convenient to represent the state variables in complex notation

$$\begin{aligned} S_i(x_j,t) &= \hat{S}_i(x_j)\cos[\omega t+\phi_{S_i}(x_j)] \\ &= \Re\{\hat{S}_i(x_j)e^{[j\omega t+\phi_{S_i}(x_j)]}\} \\ &= \Re\{\underline{\hat{S}}_i(x_j)e^{j\omega t}\}, \end{aligned} \tag{3.43}$$

where $\hat{S}_i(x_j)$ is the real amplitude and

$$\underline{\hat{S}}_i(x_j)=\hat{S}_i(x_j)e^{j\phi_{S_i}(x_j)} \tag{3.44}$$

the complex amplitude, including the phase angle ϕ_{S_i}. A corresponding notation could be adopted for the T_i, E_k and D_k, but for simplicity the extra hats

and underlines shall be omitted and all time dependent quantities will be substituted by their complex amplitudes. In this complex representation, POYNTING's theorem for a piezoelectric body is found to be [AUL89]

$$\int_S P_i n_i \,\mathrm{d}S = j\omega \frac{1}{2} \int_V (T_i S_i^* + E_k D_k^* - \rho v_i v_i^*) \,\mathrm{d}V - \frac{1}{2} \int_V F_i v_i^* \,\mathrm{d}V, \tag{3.45}$$

where P_i is the complex POYNTING vector

$$P_i = \frac{1}{2} \left[\phi \left[j\omega D_i \right]^* + P_i^{(\mathrm{m})} \right] \tag{3.46}$$

and n_i the outward unit normal vector on the surface of the body. The integrations are carried out over the surface S and the volume V of the body, the asterisk denotes the conjugate of the complex amplitudes. Elastic contributions $P_i^{(\mathrm{m})}$ to the complex power flow cannot be represented in the engineering notation used here. In standard tensor notation they are $P_i^{(\mathrm{m})} = -T_{ij} v_j^*$.

The integral terms on the right hand side of (3.45) can be identified as

$$\begin{aligned} U_{\mathrm{peak}} &= \frac{1}{2} \int_V (T_p S_p^* + E_k D_k^*) \,\mathrm{d}V, \\ T_{\mathrm{peak}} &= \frac{1}{2} \int_V \rho v_i v_i^* \,\mathrm{d}V, \end{aligned} \tag{3.47}$$

the peak potential and kinetic energy of the system, respectively. Obviously, T_{peak} is a real expression and U_{peak} is also real, provided the constitutive relations satisfy

$$\begin{bmatrix} S_p \\ D_k \end{bmatrix}^* = \begin{bmatrix} s_{pq}^E & d_{pl} \\ d_{kq} & \varepsilon_{kl}^T \end{bmatrix} \begin{bmatrix} T_q \\ E_l \end{bmatrix}^*, \tag{3.48}$$

which is true, if the matrix of the constitutive coefficients is real and symmetric. If the body is free of volume forces F_i, POYNTING's theorem can be written as

$$\frac{1}{2} \int_S \left[\phi \left[j\omega D_i \right]^* + P_i^{(\mathrm{m})} \right] n_i \,\mathrm{d}S = j\omega (U_{\mathrm{peak}} - T_{\mathrm{peak}}), \tag{3.49}$$

and it is seen, that expressions on both sides are imaginary quantities.

Energy conversion in lossless piezoelectric media is represented by (3.49) as the real part of the power flow $P_i n_i$ across the surface of the considered volume. If it is assumed, that stresses T_{ij} and surface charge density $\sigma = -D_i n_i$ are present on distinct surfaces S_T and S_σ only, the real part of (3.49) becomes

$$\frac{1}{2} \Re \left\{ \int_{S_\sigma} \phi \left[j\omega D_i \right]^* n_i \,\mathrm{d}S \right\} + \frac{1}{2} \Re \left\{ \int_{S_T} P_i^{(\mathrm{m})} n_i \,\mathrm{d}S \right\} = 0, \tag{3.50}$$

and if S_T and S_σ are identified as the mechanical and electrical ports of the system, this simply states that resistive power flow through the mechanical port equals minus the resistive power flow through the electrical port.

In the following analysis, energy conversion from the electrical to the mechanical port of the system shall be considered. The piezoelectric laminate (fig. 3.1) is excited by a harmonic voltage $\Delta\phi = V(t) = V_0 e^{j\Omega t}$. At the electrical port, the complex power input is then

$$P_{\mathrm{el}} = \frac{1}{2}\int_{S_\sigma} \phi\,[j\omega D_i]^* n_i \,\mathrm{d}S \tag{3.51}$$

where the integration has to be carried out over the electroded top and bottom surfaces corresponding to S_σ. The dielectric displacement D_i is given by (3.17) leading to

$$P_{\mathrm{el}} = \frac{1}{2}V_0 j\Omega bL\left[(1-k_{31}^2)\varepsilon_{33}^T\frac{V_0}{h} + \frac{d_{31}}{s_{11}^E}(e+\frac{h}{2})\frac{1}{L}w'|_0^L\right]^* = \frac{1}{2}V_0 I_0^*, \tag{3.52}$$

where the factor multiplied by $\frac{1}{2}V_0$ can be recognized as the conjugate of the complex amplitude I_0 of the current

$$I(t) = I_0 e^{j\Omega t} = -j\Omega bL\left[(1-k_{31}^2)\varepsilon_{33}^T\frac{V_0}{h} + \frac{d_{31}}{s_{11}^E}(e+\frac{h}{2})\frac{1}{L}w'|_0^L\right]e^{j\Omega t} \tag{3.53}$$

which depends on the applied voltage V_0 and the resulting displacement $w(x_1)$ of the laminate. The work W_{conv} that is converted from the electrical to the mechanical port per harmonic deformation cycle is proportional to the *resistive power*, which is the real part of the electric power, according to

$$W_{\mathrm{conv}} = \frac{2\pi}{\Omega}\Re\{P_{\mathrm{el}}\}, \tag{3.54}$$

and obviously this expression corresponds to U_{conv} in the definition of the EMCF (2.42) which is based on a quasi-static cycle of deformation and discharge. Now, to come up with a similar definition for harmonic cycles, a corresponding expression for U_{oc} or in MASON's words *"the total input electrical energy obtained from the input battery"* must be found. For harmonic cycles, where energy transfer is continuous rather than sequential as in the case of the quasi-static cycle, the maximum of the work supplied in one cycle is dependent on the choice of the start/end point of the cycle. This is a typical problem encountered in the treatment of alternating or arbitrary time dependent currents and voltages and

it is customary to represent these time dependent quantities by their *effective* values, defined as

$$\bar{I}^2 = \frac{1}{T}\int_0^T I^2(t)\,\mathrm{d}t, \tag{3.55}$$

where T is typically the period, but can also go to infinity for nonperiodic signals. The *apparent* power is the product of the effective voltage and current so that for harmonic signals

$$\bar{V}\bar{I} = \frac{1}{2}\,|V_0 I_0^*| = |P_{\mathrm{el}}| \tag{3.56}$$

and the work expression resulting from the apparent power will be considered equivalent to the maximum work supplied from the electric power source in one cycle, which is clearly different from the converted work (3.54). Rather than taking the ratio of the time averaged converted and maximum work, the ratio of the corresponding power expressions

$$\frac{\Re\{P_{\mathrm{el}}\}}{|P_{\mathrm{el}}|} = \frac{\Re\{V_0 I_0^*\}}{|V_0 I_0^*|} = \cos\phi, \tag{3.57}$$

is taken, where ϕ is the phase lag between voltage and current. This ratio, which is also termed the *power factor*, is consequently the equivalent to the EMCF for harmonic stationary load cycles. In some technical applications, reactive currents can become quite large compared to resistive currents, which are in phase with the applied voltage, leading to small power factors. This is undesired because the resistive losses are proportional to the square of the current and efforts are made to compensate reactive contributions by added capacitors or inductors to maximize the power factor.

The current (3.53) can be separated into two distinct contributions. The dielectric current

$$I_{\mathrm{d}} = -j\Omega b L \varepsilon_{33}^T \frac{V_0}{h}(1 - k_{31}^2), \tag{3.58}$$

is independent of the deformation of the body, corresponding to the capacitive behavior of a clamped ($S_i = 0$) piezoelectric actuator and always purely reactive if the piezoelectric layer is free of dielectric losses. It does not contribute to the resistive power. The piezoelectric current

$$I_{\mathrm{p}} = -j\Omega b L \frac{d_{31}}{s_{11}^E}(e + \frac{h}{2})\frac{1}{L} w'|_0^L, \tag{3.59}$$

will depend on the unknown complex rotation amplitude $w'(x_1)$ of the cross-sections at the boundary $x_1 = 0$ and $x_1 = L$ of the laminate, which is proportional to the applied voltage V_0. The piezoelectric current can be expressed as

a function of

$$\frac{1}{L} w'|_0^L = V_0 \Psi, \tag{3.60}$$

where Ψ is a complex valued function of the frequency of excitation Ω. Without loss of generality, V_0 can be assumed real, and the power factor (3.57) is entirely determined by the complex current amplitude I_0. Provided, the resistive power $\Re\{P_{\mathrm{el}}\}$ is positive, finding a maximum of the power factor is equivalent to minimizing the expression

$$\left[\frac{\Im\{P_{\mathrm{el}}\}}{\Re\{P_{\mathrm{el}}\}}\right]^2 = \frac{1}{\Im\{\Psi\}^2}\left[\frac{d_{31}(1-k_{31}^2)}{k_{31}^2(e+\frac{h}{2})h} + \Re\{\Psi\}\right]^2 \tag{3.61}$$

and further analysis of this expression is not promising without consideration of the influence of the thickness h of the piezoelectric layer on the complex steady state response $w(x_1)$ of the forced vibration problem. Again, explicit solutions for the equations of motion can only be found for very simple configurations. For reasonably complex systems, the optimal geometry of a piezoelectric actuator can be determined based on numerical solutions. This is demonstrated in chapter four.

The concept of the determination of the optimal actuator design and location based on the actuator power factor was also introduced by Liang, Sun, Zhou and Rogers [ZR95], [LSR95]. They justified the use of the actuator power factor, defined as the ratio

$$\psi = \frac{\text{Dissipative Mechanical Power}}{\text{Supplied Electrical Power}} = \frac{\Re\{Y_s\}}{|Y_s|}, \tag{3.62}$$

where Y_s is the electrical admittance of the actuator, by general impedance considerations [LSR97] rather than the demonstrated analogy to the EMCF.

Chapter 4

Verification

4.1 EMCF: Theory versus Finite Element Model for a periodic system

There is a variety of finite element codes capable of modeling coupled field interactions, including the piezoelectric effect. The ANSYS finite element package has been used to compute resonance and antiresonance frequencies $f_{\mathrm{r}}, f_{\mathrm{a}}$ of the periodic laminate beam (fig. 3.2) for different thickness ratios H/h. The geometry of the beam is discretized into quadrilateral 2D elements (fig. 4.1). Displacement degrees of freedom are coupled at the periodic boundaries, voltage degrees of freedom are coupled along the electrode and the boundary to the non piezoelectric substrate layer, respectively.

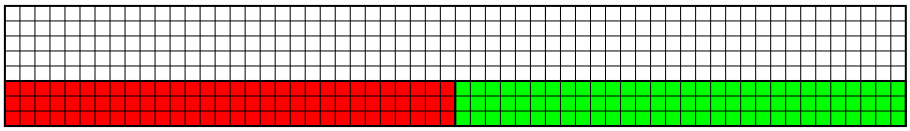

Figure 4.1: finite element mesh for the periodic laminate beam

A modal analysis has been carried out for resonance (fixed zero potential) and antiresonance (free potential) electric boundary conditions, which are applied on the electrode and the boundary between piezoelectric and substrate layer. From the computed eigenfrequencies, the dynamic EMCF (2.57) was calculated and plotted over the thickness ratio h/H of the laminate beam for two different substrate materials and two different aspect ratios L/h (figs. 4.2 and

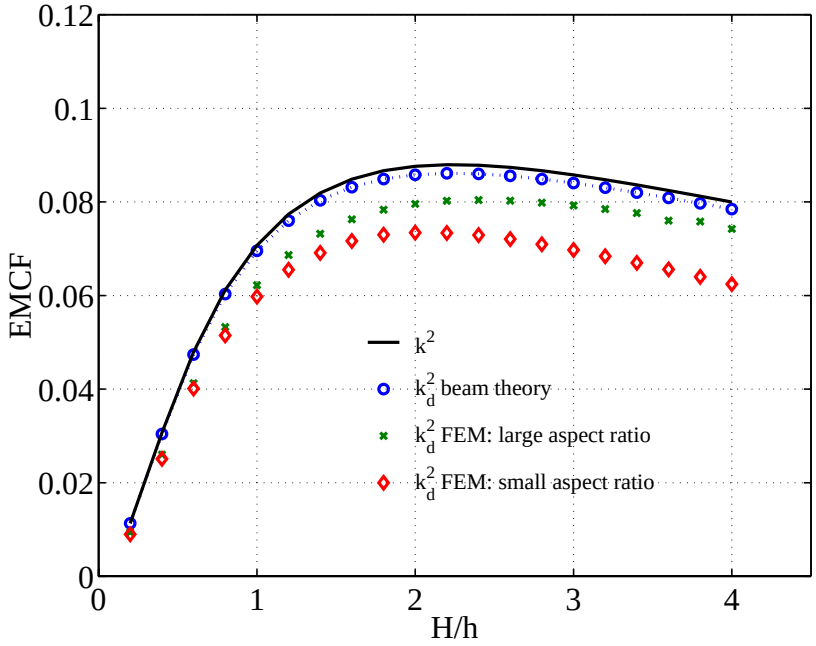

Figure 4.2: EMCF over thickness ratio H/h; substrate: aluminum

4.3). The solid curves show the EMCF according to definition (2.42) determined analytically for a prescribed harmonic (sinusoidal) mode of deformation of the laminate. Circles represent values of the dynamic EMCF calculated from eqns. (3.41) and (3.39). Stars and diamonds are finite element results of the dynamic EMCF for large and small aspect ratio.

The available 2D elements are restricted to plane strain models so the material constants used for analytical computation of the EMCF and dynamic EMCF for the considered uniaxial stress in the BERNOULLI-EULER laminate had to be adapted to give plane strain results. Based on the representation used in the finite element package, where (S_i, E_i) are independent variables, taking into consideration that the laminate is free of shear deformation and of the electrical quantities, only the ones in the direction of polarization are of interest, constitutive equations in the form

$$\begin{aligned} T_1 &= c_{11}^E S_1 + c_{12}^E S_2 + c_{13}^E S_3 - e_{31} E_3, \\ T_2 &= c_{12}^E S_1 + c_{11}^E S_2 + c_{13}^E S_3 - e_{31} E_3, \\ T_3 &= c_{13}^E (S_1 + S_2) + c_{33}^E S_3 - e_{33} E_3, \\ D_3 &= e_{31} (S_1 + S_2) + e_{33} S_3 + \varepsilon_{33}^S E_3, \end{aligned} \tag{4.1}$$

are obtained for the BERNOULLI-EULER laminate. In addition, the strain S_2 in

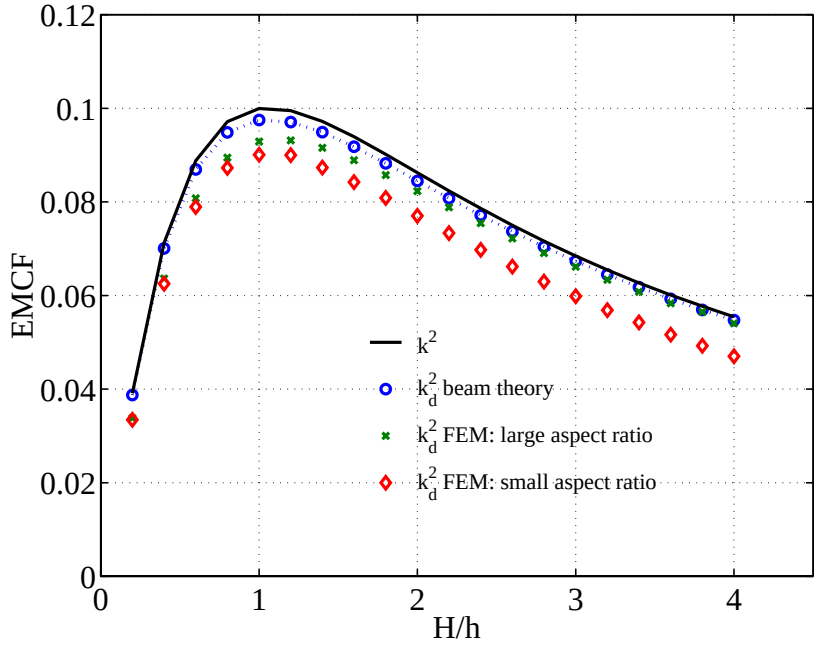

Figure 4.3: EMCF over thickness ratio H/h; substrate: steel

width direction and the stress T_3 in thickness direction vanish. Solving (4.1) for (S_1, D_3) leads to constitutive equations

$$\begin{aligned} S_1 &= \frac{1}{c_{11}^E c_{33}^E - c_{13}^E c_{13}^E} \left[c_{33}^E T_1 - \left(c_{13}^E e_{33} - c_{33}^E e_{31} \right) E_3 \right], \\ D_3 &= \frac{1}{c_{11}^E c_{33}^E - c_{13}^E c_{13}^E} \Big[(c_{13}^E e_{33} - c_{33}^E e_{31}) T_1 \\ &+ \left[c_{13}^E c_{13}^E \varepsilon_{33}^S + 2 c_{13}^E e_{31} e_{33} - c_{33}^E (e_{31}^2 + c_{11}^E \varepsilon_{33}^S) - c_{11}^E e_{33}^2 \right] E_3 \Big], \end{aligned} \quad (4.2)$$

which are of the form (3.4), (3.5). These are suitable to obtain analytical results from the expressions derived for the laminate in chapter three to be compared with plane strain finite element computations.

As it is evident from table 4.1, the computed analytical and numerical results for resonance and antiresonance frequencies are very close. Still, there is a noticeable difference in the values obtained for the dynamic EMCF, as the frequency based formula (3.42) is very sensitive to frequency deviations.

Figure (4.4) shows an example of resonance and antiresonance modes of vibration of the bulky periodic laminate beam, for a thickness ratio H/h of two.

	Analysis			FEM		
H/h	f_r [Hz]	f_a [Hz]	k_d^2	f_r [Hz]	f_a [Hz]	k_d^2
2.0	598.548	625.559	0.0844	598.088	624.333	0.0823
2.2	643.589	671.268	0.0807	643.019	669.974	0.0788
2.4	689.236	717.468	0.0771	688.525	716.069	0.0755
2.6	735.397	764.091	0.0736	734.515	762.552	0.0722
2.8	781.997	811.079	0.0704	780.908	809.360	0.0691
3.0	828.972	858.383	0.0673	827.643	856.447	0.0661

Table 4.1: resonance and antiresonance frequencies for the periodic laminate beam

The deformation is very similar, but the electric potential distribution, represented by isopotential lines, in the piezoelectric layer is quite different for the two modes. For the periodic Bernoulli-Euler laminate, the piezoelectric current (3.59) is purely reactive as no energy is dissipated or transformed and is either in phase or 180° out of phase with the dielectric current (3.58). Antiresonance frequencies are generally higher and for this system only little higher than the corresponding resonance frequencies.

When piezoelectric and dielectric current are in phase slightly below resonance, they will be opposite in sign slightly above resonance. Under antiresonance conditions these two contributions compensate each other and it is no surprise that resonance and antiresonance modes can be so similar. It is not the case, that the particular strain distribution of the antiresonance mode would lead to zero piezoelectric current.

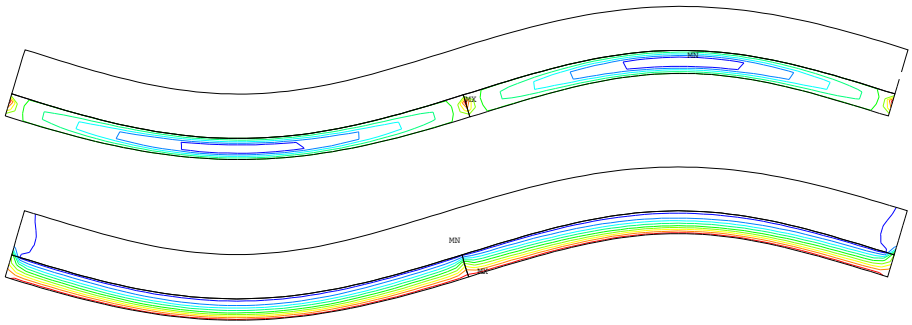

Figure 4.4: resonance (top) and antiresonance (bottom) eigenmode of the laminated periodic beam; isopotential lines represent the electric potential distribution in the piezoelectric layer

4.2 Power Factor: Theory versus Experiment for an infinite beam

In the previous chapter, analytical investigations aimed at finding an optimal thickness of the piezoelectric layer without solving the equations of motion for a particular actuator application. This has been partially successful in the case of the EMCF, where optimum thickness ratios could be given based on a hypothetical prescribed cycle of deformation. For the power factor as optimization variable this was not possible in this general way and in this section optimal dimensions of piezoelectric bending actuators shall be determined based on numerical solutions of the equations of motion. To verify the predictions of the mathematical model, numerical results are compared to measured data obtained from an experimental setup [STÖ98].

4.2.1 The problem geometry

Continuous transfer of resistive power into an electromechanical system requires either some kind of dissipation mechanism or boundary conditions, which allow for energy transfer across the boundaries of the system. The geometry here considered is a piezoelectric patch bonded to an infinite beam (fig. 4.5), which was also suggested by GIBBS and FULLER, who investigated simultaneous actuation of flexural and longitudinal waves for actuator pairs on infinite beams [GF92].

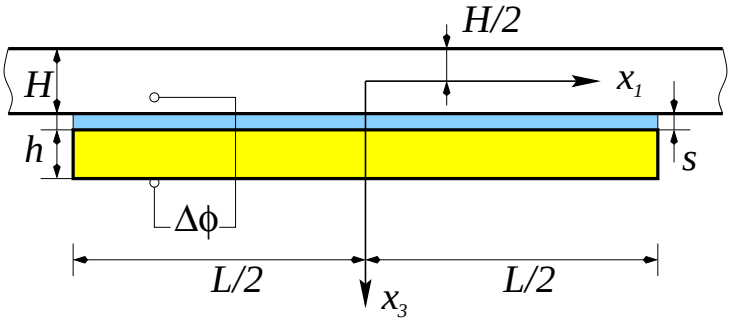

Figure 4.5: piezoelectric patch bonded to infinite beam

4.2.2 Model for the bonded actuator

For the kinematical model of the single bonded actuator (fig. 4.6), the piezoelectric patch and the substrate beam are assumed to undergo bending as well as

longitudinal deformation. The bonding layer is shear elastic but rigid in thickness direction and therefore allows for relative longitudinal displacement of the bonded surfaces of the actuator and substrate layer. A kinematic relation for

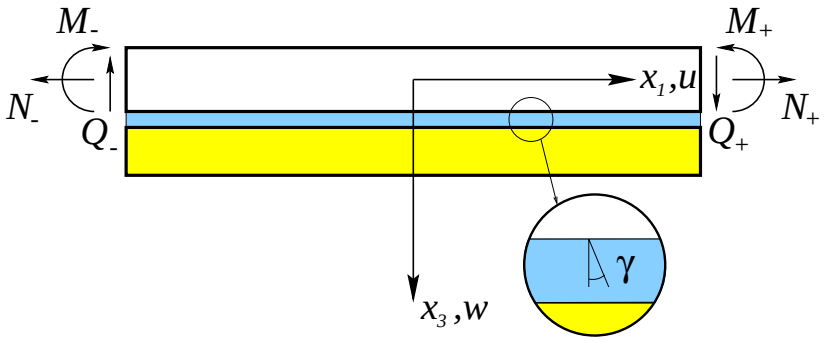

Figure 4.6: laminate section with boundary forces/moments

the displacement corresponding to these assumptions is obtained as

$$\begin{aligned} u_{\mathrm{s}}(x_1, x_3, t) &= u(x_1, t) - x_3 w'(x_1, t), \\ u_{\mathrm{p}}(x_1, x_3, t) &= u(x_1, t) - x_3 w'(x_1, t) + s\gamma(x_1, t), \end{aligned} \tag{4.3}$$

where the two dimensional fields $u_{\mathrm{s}}(x_1, x_3, t), u_{\mathrm{p}}(x_1, x_3, t)$ of the displacement in longitudinal (x_1) direction for the substrate and the piezoelectric layer, respectively, are represented by the one dimensional fields $w(x_1, t)$, for the transverse displacement of the entire laminate in x_3 direction, $u(x_1, t)$ for the longitudinal displacement of the middle layer of the substrate beam and $\gamma(x_1, t)$, the shear angle of the thin bonding layer, which is assumed constant over the thickness s of the layer.

Based on the kinematic relation (4.3), potential and kinetic energies of the laminate section can be expressed in terms of the independent variables $u(x_1, t), w(x_1, t)$ and $\gamma(x_1, t)$. For the kinetic energy density $T_{\mathrm{s}}(x_1, t)$ of the substrate, the expression

$$T_{\mathrm{s}}(x_1, t) = \frac{1}{2}\rho_{\mathrm{s}} \left[\dot{u}^2(x_1, t) + \dot{w}^2(x_1, t)\right] \tag{4.4}$$

is obtained where terms proportional to $\dot{w}'$, which represent the rotational energy of the cross-sections of the beam and patch are neglected. The potential energy density becomes

$$U_{\mathrm{s}}(x_1, x_3, t) = \frac{1}{2} E_{\mathrm{s}}\, u_{\mathrm{s}}'^2(x_1, x_3, t). \tag{4.5}$$

As the mass density of the bonding layer is small compared to the other layers,

its kinetic energy contribution is neglected and only the potential energy density

$$U_{\mathrm{b}}(x_1,t) \;=\; \frac{1}{2} G_{\mathrm{b}}\, \gamma^2(x_1,t), \tag{4.6}$$

stored in shear deformation is taken into account. In the piezoelectric patch, the kinetic energy density

$$T_{\mathrm{p}}(x_1,t) \;=\; \frac{1}{2}\rho_{\mathrm{p}} \left[(\dot{u}(x_1,t) \;+\; s\,\dot{\gamma}(x_1,t))^2 \;+\; \dot{w}^2(x_1,t) \right] \tag{4.7}$$

contains additional terms in $\dot{\gamma}$ due to the shear elasticity of the bonding layer. Again, as for the substrate layer, rotational energy terms in $\dot{w}'$ are neglected.

With the constitutive equations (3.4), (3.5) for the piezoelectric layer and the displacement field (4.3), following the derivation given in chapter three, the electric field

$$E_3(x_1,x_3,t) \;=\; \frac{k_{31}^2}{d_{31}(1-k_{31}^2)} \left[x_3 - \frac{h+2s+H}{2} \right] w''(x_1,t) - \frac{\Delta\phi(t)}{h} \tag{4.8}$$

is again a linear function of the thickness coordinate x_3 and proportional to both, the applied voltage $\Delta\phi(t)$ and the curvature $w''(x_1,t)$ of the laminate section. The electric enthalpy density H_{p} of the piezoelectric layer corresponding to (3.33) can now be expressed in displacement (u, w, γ) and electric potential ϕ as the independent quantities, however, the resulting expression is rather bulky and will not be given here. The resulting LAGRANGEian of the laminate section

$$L = \int_V (T_{\mathrm{p}} + T_{\mathrm{s}} - H_{\mathrm{p}} - U_{\mathrm{s}} - U_{\mathrm{b}})\, \mathrm{d}V$$

with displacements and electric potential as the independent variables is suitable for substitution into (2.18).

For a state change $\delta u, \delta w$ of the laminate section, the virtual work of the external forces done on the laminate is

$$\delta W \;= Q_+\delta w_+ + N_+\delta u_+ - M_+\delta w'_+ - N_-\delta u_- - Q_-\delta w_- + M_-\delta w'_-\,, \tag{4.9}$$

where the bending moment M, the shear force Q, the normal force N and the corresponding rotations and displacements w', w and u in the substrate beam are evaluated at the boundaries of the laminate section in positive $(+)$ and negative $(-)$ x_1 direction, which is indicated by the subscripts. The virtual work of the external charges in expression (2.17) is zero as for the given prescribed potential boundary conditions no arbitrary variation of the potential on the electrodes is permitted. Consequently, (4.9) represents the total virtual work done on the

laminate section and can be substituted together with the LAGRANGEian (4.2.2) into HAMILTON's principle (2.18). After partial integration and collection of terms in the same independent variations, the equations of motion of the system are obtained. So far, the forces N, Q and bending moment M at the boundaries of the laminate section are still unknown.

A single piezoelectric patch on an infinite beam can be thought of as a laminate section (fig. 4.6) connected to two semi-infinite beams. For the steady state response to harmonic voltage excitation $\Delta\phi = V_0 \cos \Omega t$, force and bending moment amplitudes at the boundary of the laminate section can then be determined in complex representation from a dynamic stiffness matrix for the semi-infinite beam [CH88] according to

$$\begin{pmatrix} \hat{\underline{Q}}_+ \\ \hat{\underline{M}}_+ \\ \hat{\underline{N}}_+ \end{pmatrix} = \begin{bmatrix} \underline{b}_{11+} & \underline{b}_{12+} & 0 \\ \underline{b}_{21+} & \underline{b}_{22+} & 0 \\ 0 & 0 & \underline{b}_{33+} \end{bmatrix} \begin{pmatrix} \hat{\underline{w}}_+ \\ \hat{\underline{w}}'_+ \\ \hat{\underline{u}}_+ \end{pmatrix}, \tag{4.10}$$

where the complex coefficients $\underline{b}_{ij+}$ are frequency dependent. For the semi-infinite beam, the $\underline{b}_{ij+}$ become

$$\begin{aligned} \underline{b}_{11+} &= (-1+j) EI k_w^3, \\ \underline{b}_{12+} &= -jEIk_w^2, \\ \underline{b}_{21+} &= -\underline{b}_{12+}, \\ \underline{b}_{22+} &= (1+j) EI k_w, \\ \underline{b}_{33+} &= j\Omega A \sqrt{\rho E}, \end{aligned} \tag{4.11}$$

where E is YOUNG's modulus, I the moment of inertia of the cross-section and A the cross-sectional area of the substrate beam. For the second boundary, the coefficients b_{ij-} may differ only in the sign, depending on the choice of the coordinate frame x_i and the orientation of forces Q, N and bending moment M. The dispersion relation

$$k_w^4 = \Omega^2 \frac{\rho A}{EI}$$

for flexural waves relates the wavenumber k_w to the frequency of vibration, with ρ as the mass density of the substrate beam.

The steady state response of a finite beam excited by a piezoelectric patch can be modeled by connecting finite length beam ends to the laminate section. For a finite beam of length l_s, the corresponding b_{ij+} of the dynamic stiffness matrix are

$$\underline{B} = 1 + e^{2\,j\,k_w\,l_\mathrm{s}} + 4\,e^{(1+j)k_w\,l_\mathrm{s}} + e^{2\,k_w\,l_\mathrm{s}} + e^{(2+2\,j)\,k_w\,l_\mathrm{s}},$$

$$
\begin{aligned}
\underline{b}_{11+} &= \frac{1}{\underline{B}}\,(1+j)(-j+e^{2\,j\,k_w\,l_\mathrm{s}}-e^{2\,k_w\,l_\mathrm{s}}+j\,e^{(2+2\,j)k_w\,l_\mathrm{s}})EI\,k_w^3,\\
\underline{b}_{12+} &= \frac{1}{\underline{B}}\,j(-1+e^{2\,j\,k_w\,l_\mathrm{s}})(-1+e^{2\,k_w\,l_\mathrm{s}})EI\,k_w^2,\\
\underline{b}_{21+} &= -\underline{b}_{12+},\\
\underline{b}_{22+} &= \frac{1}{\underline{B}}\,(1+j)(-1+j\,e^{2\,j\,k_w\,l_\mathrm{s}}-j\,e^{2\,k_w\,l_\mathrm{s}}+e^{(2+2\,j)k_w\,l_\mathrm{s}})EI\,k_w,\\
\underline{b}_{33+} &= -\Omega A\sqrt{\rho E}\,\tan\left[\Omega l_\mathrm{s}\sqrt{\frac{\rho}{E}}\,\right],
\end{aligned}
\tag{4.12}
$$

and for the b_{ij-} again, only the sign may be different.

In either case, for semi-infinite or finite beam ends, the unknown Q, M, N at the boundaries of the laminate section can be expressed by the independent displacement quantities w, u and after separation of time, according to

$$
\begin{aligned}
\gamma(x_1,t) &= \Re\{\underline{\Gamma}(x_1)e^{j\Omega t}\},\\
u(x_1,t) &= \Re\{\underline{U}(x_1)\,e^{j\Omega t}\},\\
w(x_1,t) &= \Re\{\underline{W}(x_1)\,e^{j\Omega t}\},
\end{aligned}
\tag{4.13}
$$

a system of three coupled equations of motion in the form

$$
\begin{aligned}
c_1\,\underline{\Gamma}+c_5\,\Omega^2\,\underline{U}+c_6\,\Omega^2\,\underline{\Gamma}-c_{11}\,\underline{U}'-c_{12}\,\underline{\Gamma}''-c_{13}\,\underline{W}''' &= 0,\\
c_2\,\Omega^2\,\underline{U}+c_3\,\Omega^2\,\underline{\Gamma}-c_7\,\underline{U}''-c_8\,\underline{\Gamma}''-c_9\,\underline{W}''' &= 0,\\
c_4\,\Omega^2\,\underline{W}+c_{15}\,\underline{U}'''+c_{16}\,\underline{\Gamma}'''+c_{17}\,\underline{W}^{IV} &= 0,
\end{aligned}
\tag{4.14}
$$

with inhomogeneous boundary conditions

$$
\left.
\begin{aligned}
-c_7\,\underline{U}'-c_8\underline{\Gamma}'-c_9\,\underline{W}''+\underline{b}_{33}\,\underline{U} &= c_{10}\,V_0\\
-c_{11}\,\underline{U}'-c_{12}\,\underline{\Gamma}'-c_{13}\,\underline{W}'' &= c_{14}\,V_0\\
-c_{15}\,\underline{U}'-c_{16}\,\underline{\Gamma}'-c_{17}\,\underline{W}''+\underline{b}_{21}\,\underline{W}+\underline{b}_{22}\,\underline{W}' &= c_{18}\,V_0\\
c_{15}\,\underline{U}''+c_{16}\,\underline{\Gamma}''+c_{17}\,\underline{W}'''+\underline{b}_{11}\,\underline{W}+\underline{b}_{12}\,\underline{W}' &= 0
\end{aligned}
\right|_{x_1=+\frac{L}{2}},
\tag{4.15}
$$

$$
\left.
\begin{aligned}
-c_7\,\underline{U}'-c_8\underline{\Gamma}'-c_9\,\underline{W}''-\underline{b}_{33}\,\underline{U} &= c_{10}\,V_0\\
-c_{11}\,\underline{U}'-c_{12}\,\underline{\Gamma}'-c_{13}\,\underline{W}'' &= c_{14}\,V_0\\
-c_{15}\,\underline{U}'-c_{16}\,\underline{\Gamma}'-c_{17}\,\underline{W}''+\underline{b}_{21}\,\underline{W}-\underline{b}_{22}\,\underline{W}' &= c_{18}\,V_0\\
c_{15}\,\underline{U}''+c_{16}\,\underline{\Gamma}''+c_{17}\,\underline{W}'''-\underline{b}_{11}\,\underline{W}+\underline{b}_{12}\,\underline{W}' &= 0
\end{aligned}
\right|_{x_1=-\frac{L}{2}},
$$

is found. The constants c_{1-18}

$$
\begin{aligned}
c_1 &= -b\,G_K\,s,\\
c_2 &= b(h\,\rho_P + H\,\rho_S),\\
c_3 &= b\,s\,h\,\rho_P,\\
c_4 &= b(h\,\rho_P + H\,\rho_S),\\
c_5 &= b\,s\,h\,\rho_P,\\
c_6 &= b\,s^2\,h\,\rho_P,\\
c_7 &= -b\,(H\,E_S + h/s_{11}^E),\\
c_8 &= -b\,s\,h/s_{11}^E,\\
c_9 &= b\,h\frac{h+H+2\,s}{2\,s_{11}^E},\\
c_{10} &= -b\,d_{31}/s_{11}^E,\\
c_{11} &= -b\,s\,h/s_{11}^E,\\
c_{12} &= c_{11}\,s,\\
c_{13} &= b\,s\,h\frac{h+H+2\,s}{2\,s_{11}^E},\\
c_{14} &= -b\,s\,d_{31}/s_{11}^E,\\
c_{15} &= h\,b\frac{h+H+2\,s}{2\,s_{11}^E},\\
c_{16} &= s\,c_{15},\\
c_{17} &= -b(h^3(-4+3\,k_{31}^2)+3\,h(-1+k_{31}^2)(H+2\,s)(2\,h+H+2\,s)+\\
&\quad E_S\,H^3\,(-1+k_{31}^2)\,s_{11}^E)/(12\,(-1+k_{31}^2)\,s_{11}^E),\\
c_{18} &= b\,\frac{d_{31}(2\,e+h)}{2\,s_{11}^E}
\end{aligned}
\tag{4.16}
$$

for the infinite beam contain material and geometrical parameters of the system.

For the solution of the coupled system (4.14) in $\underline{U}$, $\underline{\Gamma}$ and $\underline{W}$ the ansatz

$$
\begin{aligned}
\underline{U}(x_1) &= \underline{\tilde{U}}\,e^{\lambda x_1},\\
\underline{\Gamma}(x_1) &= \underline{\tilde{\Gamma}}\,e^{\lambda x_1},\\
\underline{W}(x_1) &= \underline{\tilde{W}}\,e^{\lambda x_1}
\end{aligned}
\tag{4.17}
$$

is chosen, leading to an algebraic system of equations which is represented in matrix form

$$
\boldsymbol{M}\begin{pmatrix} \underline{\tilde{U}} \\ \underline{\tilde{\Gamma}} \\ \underline{\tilde{W}} \end{pmatrix} = \mathbf{0}, \tag{4.18}
$$

with

$$\boldsymbol{M} = \begin{bmatrix} c_5\,\Omega^2 - c_{11}\,\lambda^2 & -c_{13}\,\lambda^3 & c_1 + c_6\,\Omega^2 - c_{12}\,\lambda^2 \\ c_2\,\Omega^2 - c_7\,\lambda^2 & -c_9\,\lambda^3 & c_3\,\Omega^2 - c_8\,\lambda^2 \\ c_{15}\,\lambda^3 & c_4\,\Omega^2 + c_{17}\,\lambda^4 & c_{16}\,\lambda^3 \end{bmatrix}. \tag{4.19}$$

For a nontrivial solution of the eqns. (4.18) the determinant of $\boldsymbol{M}$ must vanish

$$\det \boldsymbol{M} = 0 \tag{4.20}$$

and this characteristic equation is satisfied by each of the eight eigenvalues λ_i, $(i = 1...8)$, which are computed numerically using MATLAB. The corresponding eigenvectors

$$\underline{\boldsymbol{L}}_i = \begin{pmatrix} \underline{\tilde{U}}_i \\ \underline{\tilde{\Gamma}}_i \\ 1 \end{pmatrix} \tag{4.21}$$

are determined from (4.18) by solving the system

$$\begin{bmatrix} \text{1st row of } \boldsymbol{M}(\lambda_i) \\ \text{2nd row of } \boldsymbol{M}(\lambda_i) \end{bmatrix} \underline{\boldsymbol{L}}_i = \boldsymbol{0}, \tag{4.22}$$

where it is assumed that the first two rows of $\boldsymbol{M}(\lambda_i)$ are linearly independent[1)].

The general solution

$$\underline{\boldsymbol{L}}_{\mathrm{H}} = \sum_{i=1}^{8} \underline{C}_i\, \underline{\boldsymbol{L}}_i\, e^{\lambda_i\, x_1} \tag{4.23}$$

of the homogeneous system (4.14) is a linear combination of vectors $\underline{\boldsymbol{L}}_i$. From the inhomogeneous boundary conditions (4.15) the linear coefficients $\underline{C}_i$ are determined. These give the particular solution

$$\underline{\boldsymbol{L}}_* = \begin{pmatrix} \underline{U}_* \\ \underline{\Gamma}_* \\ \underline{W}_* \end{pmatrix} \tag{4.24}$$

of the homogeneous system (4.14) with

$$\underline{U}_* = \sum_{i=1}^{8} \underline{C}_i\, \underline{\tilde{U}}_i\, e^{\lambda_i\, x}, \tag{4.25}$$

$$\underline{\Gamma}_* = \sum_{i=1}^{8} \underline{C}_i\, \underline{\tilde{\Gamma}}_i\, e^{\lambda_i\, x}, \tag{4.26}$$

$$\underline{W}_* = \sum_{i=1}^{8} \underline{C}_i\, e^{\lambda_i\, x}. \tag{4.27}$$

[1)] If this was not the case, any other two rows of $\boldsymbol{M}(\lambda_i)$ could serve to obtain the eigenvectors.

These solutions represent the steady-state response of the actuator, from which the input electric admittance, the power factor and also the displacement of the finite or infinite beam can be computed. Due to the non-symmetrically mounted patch, longitudinal and flexural waves are coupled.

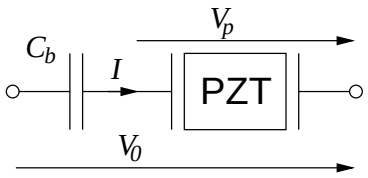

Figure 4.7: capacity C_b of the bonding layer

In other investigations of actuator patches bonded to beams, where the same patch geometry and adhesive was used [NGU99], the bonding layer was identified ideally elastic. Consequently it is modeled mechanically lossless here. Dielectric properties of the bonding material come into play as only the bottom electrode of the piezoelectric patch is connected to the power source. The conducting substrate layer serves as the second electrode and the potential on the free electrode, which is bonded to the substrate layer, depends on the capacitive influence of the bonding layer, having capacity C_b. Given the current I (fig. 4.7) the true potential difference V_p across the electrodes of the PZT patch can be computed according to

$$V_\mathrm{p} = \frac{I}{\frac{I}{V_0} + \frac{1}{j\Omega C_\mathrm{b}}} \tag{4.28}$$

where V_0 is the potential difference between bottom electrode and substrate layer.

Material loss in the actuator patch is taken into consideration here by the employment of complex values for the dielectric permittivity ε_{33}^T and the compliance s_{11}^E. Real and imaginary parts

$$\begin{aligned} {s_{11}^E}' - j\,{s_{11}^E}'' &= s_{11}^E(1 - \frac{j}{Q}) \\ {\varepsilon_{33}^T}' - j\,{\varepsilon_{33}^T}'' &= \varepsilon_{33}^T(1 - j\,\tan\delta) \end{aligned} \tag{4.29}$$

of these material parameters result from the dielectric loss $\tan\delta$ and the quality factor Q which are provided by the manufacturer of the piezoelectric patches.

Complex values for the piezoelectric constant d_{31} can be identified in experiments but they are not independent of ${s_{11}^E}''$ and ${\varepsilon_{33}^T}''$, and have to satisfy restrictions, to make sure no energy would be generated in the material [HN69].

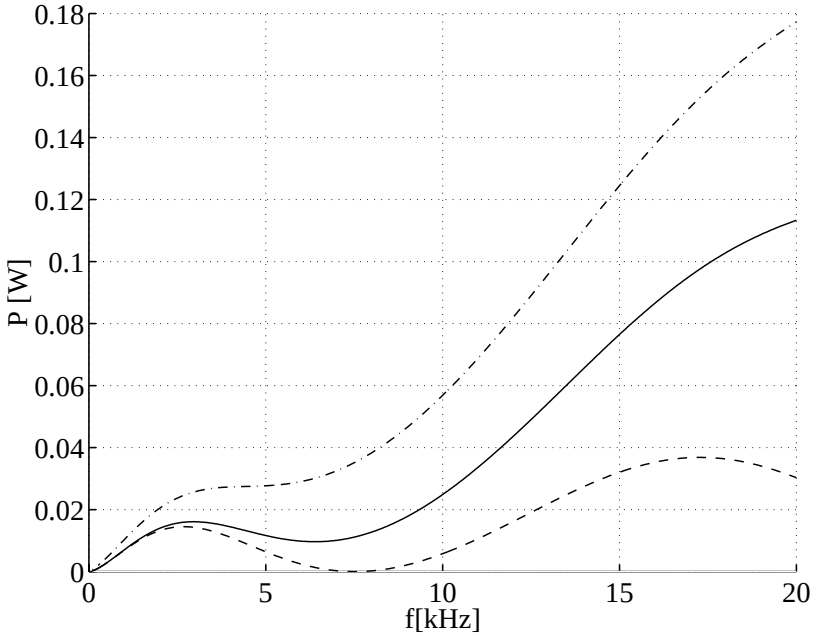

Figure 4.8: energy balance of the actuator patch on infinite beam (simulation): $(-\cdot-)$ resistive power input (electrical); (—) resistive power output (mechanical: longitudinal and flexural contributions); $(--)$ resistive power output (mechanical: only flexural waves); h=1mm, L=70mm, b=25mm, H=3mm, s=0, material: PIC 141 on steel

For this reason, and also because only Q and $\tan\delta$ were given for the piezoelectric material used in the experiments, only real values for d_{31} are employed. It turned out, that for the simulated single patch on an infinite beam, the power loss in the piezoelectric patch is in the same order of magnitude as the power that is actually converted into longitudinal and flexural waves (fig. 4.8).

4.2.3 Experimental setup

In an experimental setup, the energy transfer of single piezoelectric actuators bonded to steel beams was tested. The actuators were positioned in the center while the ends of the steel beam were embedded in sand (fig. 4.9) to avoid the reflection of flexural and also longitudinal waves, originating from the laminate region in the center of the beam. About three quarters of the beam were covered with sand, while the middle section was free.

Beams of different thicknesses (1mm, 3mm, 5mm) were tested, each approximately three meters in length and 25mm wide. Rectangular 70mm×25mm

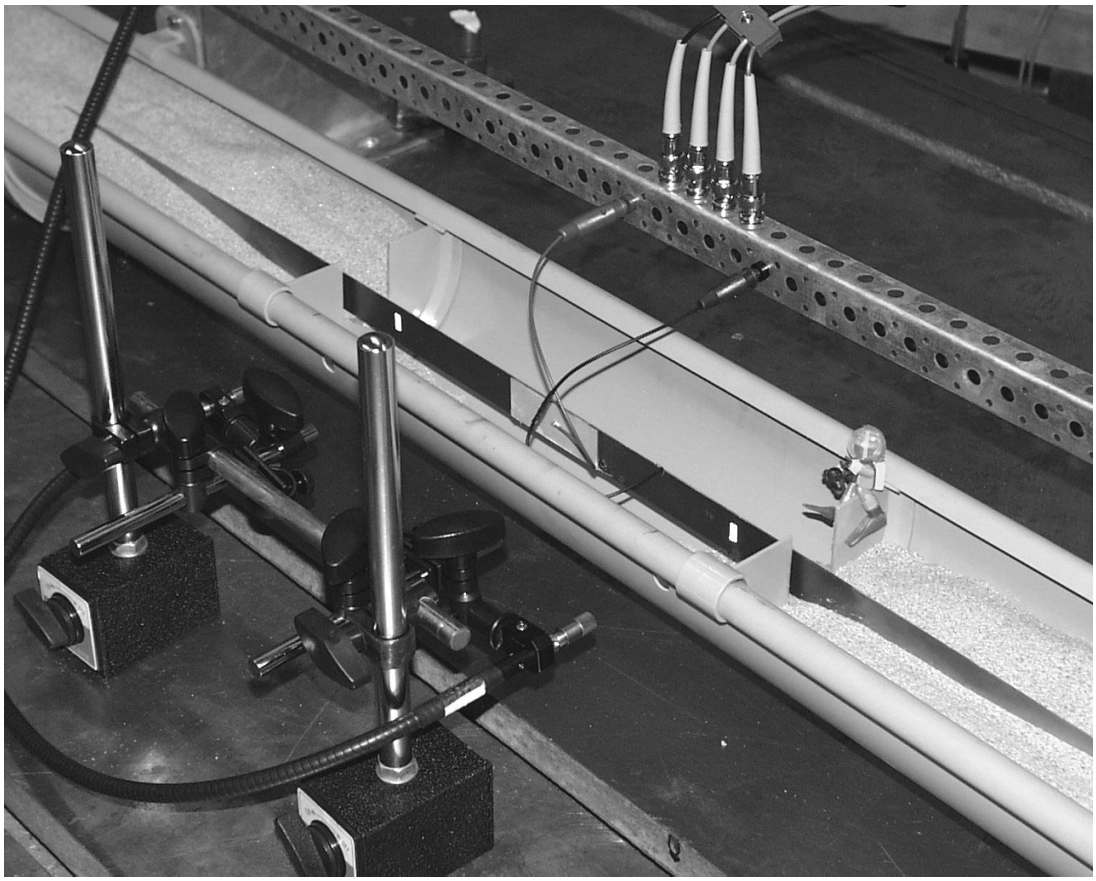

Figure 4.9: experimental setup: steel beam with ends embedded in sand

piezoelectric patches of different thicknesses (1mm, 8mm) were used, all of them made from PIC141. The material data for PIC141 is given in table 4.2. A standard cyanoacrylate fast curing adhesive[2)] was used to bond the PZT patches to the steel beams. Care must be taken to press the patch firmly against the beam surface during bonding to attain thin bond gaps. The material properties of the bonding layer were estimated[3)] to $G_{\mathrm{b}} = 3 * 10^{-7}[\frac{\mathrm{N}}{\mathrm{m}^2}]$ for the shear stiffness and $\varepsilon_{\mathrm{r}} = 4$ for the relative dielectric permittivity.

Admittance curves of the electromechanical system were measured for the free (supported by foam rubber) and embedded beam, using an impedance

[2)] LOCTITE496

[3)] Material data for this product is available on the internet at http://www.loctite.com today, but the estimated values are sufficiently close to the exact values considering that the bonding layer thickness is unknown.

PIC141 material data			
quantity	variable	value	unit
mass density	ρ_{P}	7750	$\frac{\mathrm{kg}}{\mathrm{m}^3}$
quality factor	Q	1500	1
loss tangent	$\tan\delta$	0.005	1
permittivity	ε_{33}^T	$1400 * \varepsilon_0$	$\frac{\mathrm{C}}{\mathrm{Vm}}$
compliance	s_{11}^E	$1.26 * 10^{-11}$	$\frac{\mathrm{m}^2}{\mathrm{N}}$
piez. const.	d_{31}	$-1.27 * 10^{-10}$	$\frac{\mathrm{m}}{\mathrm{V}}$

Table 4.2: material data for PIC141

analyzer[4)] at 1V output voltage. It turned out, that the longitudinal and flexural waves were damped out by the sand very well in a frequency range between 500 and 3000 Hz, so the infinite beam could be simulated in this frequency range in our experimental setup.

Fig. 4.10 shows admittance curves for the free beam. The top dashed curve is the computed absolute value $|Y|$ of the admittance for the free beam with zero bonding layer. Measured data is represented by the dotted line, from which the thickness of the bonding layer was identified, such that the solid line, the computed $|Y|$ for finite bonding layer thickness, gives as good as possible an approximation of the measurement. A thickness of $s = 2.5\mu$m was identified and it should be clear that this value, though still of a reasonable order of magnitude, will generally not be the actual thickness of the layer. However, the bonding layer thickness is the only parameter used to fit measured and calculated data, and it is unique to each bonded actuator, for all of the computations carried out. The resonance peaks in fig. 4.10 are mostly flexural modes. In the frequency range observed, only two longitudinal resonances occur for the 3m steel beam.

Fig. 4.11 shows the curves corresponding to fig. 4.10, where now the beam ends are embedded in sand and numerical results are plotted for the infinite beam model. Again, for the identified 2.5μm thickness of the bonding layer, measured (dotted line) and computed (solid line) values for $|Y|$ are in very good agreement, which is not too surprising. Apparently, longitudinal and flexural resonances are suppressed by the sand bed well enough to achieve a good approximation of the behavior of an infinite beam.

[4)] Hewlett Packard 4194A

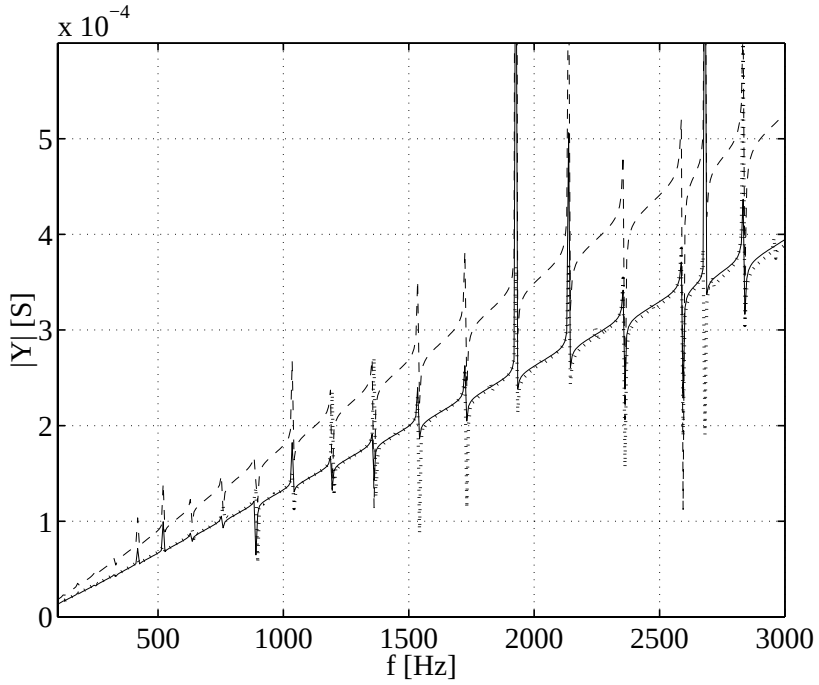

Figure 4.10: absolute value of admittance for free beam: $h = 1$mm, $H = 5$mm, $s = 2, 5\mu$m; $(--)$zero bonding layer thickness, (—)numerical data, $(\cdots)$measured data

It is rather the capacitive influence of the bonding layer than the mechanical, that causes the shift in the simulated admittance curves. Still, the mechanical aspects of the actuator's behavior are well represented. This is evident from fig. 4.12, where the computed displacement of the beam in 100mm distance from the boundary of the laminate section is plotted over the measured values for the same identified bonding layer thickness of 2.5μm. A two channel laser vibrometer[5)] was used to measure the beam displacement. The reflective stickers, which are required at the measurement points in connection with the glass fibre optics, can be seen in fig. 4.9.

In the low frequency regime, a strong deviation of measured and computed data can be observed. A possible explanation would be the near field of the bending waves originating from the discontinuity at the boundary of the laminate section. For low frequencies, these near fields reach into the sand covered area which might lead to undesired reflections and resonance phenomena. This low frequency deviation from the ideal behavior might not be evident in the admittance curves, because admittance measurements were performed at

[5)] POLYTEC OFN508/2802

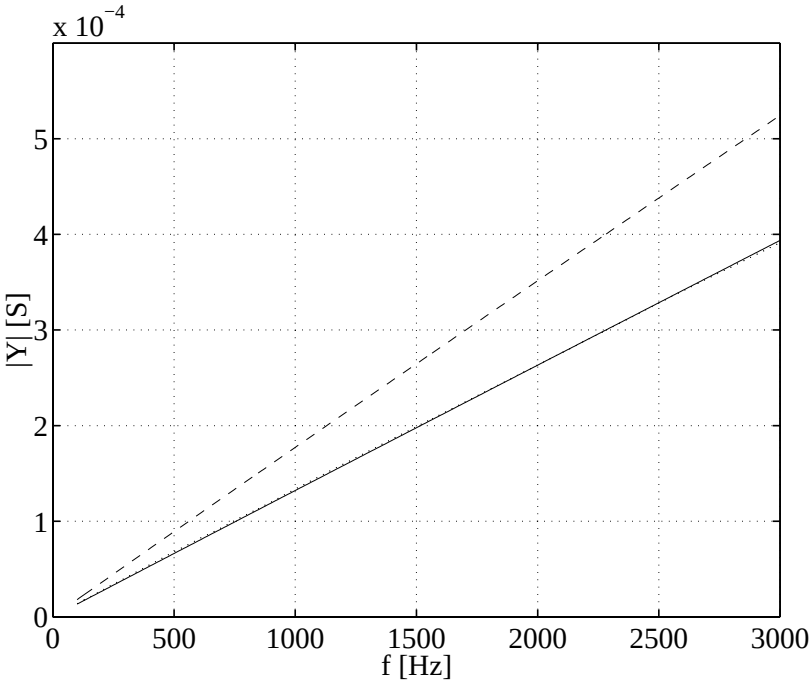

Figure 4.11: absolute value of admittance for embedded beam: $h = 1$mm, $H = 5$mm, $s = 2, 5\mu$m; $(--)$zero bonding layer thickness, (—)numerical data, $(\cdots)$measured data

1V output voltage whereas a 100V amplitude was required for the displacement measurement to obtain a reasonable signal to noise ratio for the laser vibrometer output. Above 500Hz the results are still nice.

Similar good agreement of measurements and computed results is observed for the power factor $\cos\phi$. For an 8mm PZT patch on a 3mm steel beam, measured (circles) and computed (solid line) data are plotted in fig. 4.13. The identified bonding layer thickness in this case was $s = 2.5\mu$m.

4.2.4 Optimal patch geometry

For the 70mm length actuator patches used, it was assumed they would be ideally suited to excite flexural waves of 140mm wavelength in the substrate beam. At the corresponding frequency of excitation, 1431Hz for a 3mm steel beam, the steady state response of the single patch on an infinite beam was calculated for various actuator geometries. Only the flexural wave contributions $P_{\text{out,flex}}$ to the power output were considered for the computation of the *effective bending*

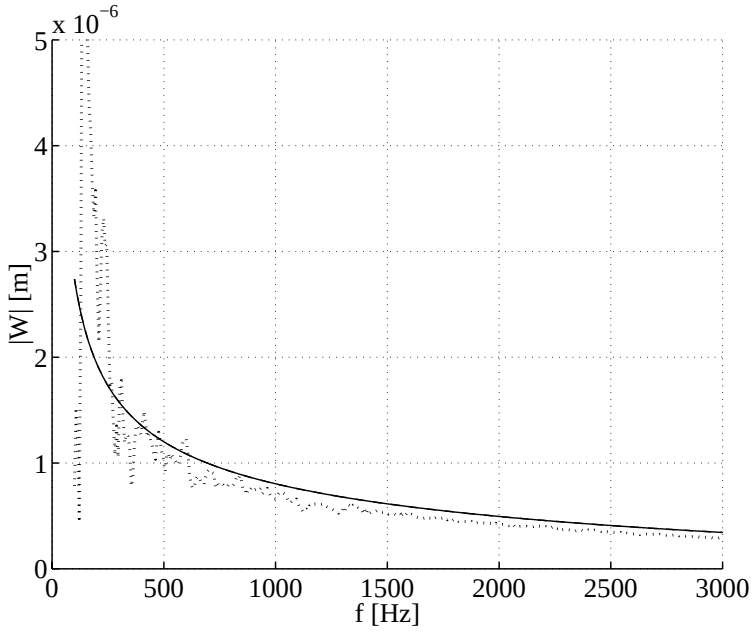

Figure 4.12: displacement $w(x_1 = 135mm)$: theory (—)and experiment $(\cdots)$

power factor κ according to

$$\kappa = \eta\nu\cos\phi = \frac{\Re\{P_{\text{out,flex}}\}}{|P_{\text{in,elec}}|}, \tag{4.30}$$

where $|P_{\text{in,elec}}|$ is the apparent electrical input power, η is the efficiency of the power conversion of the lossy actuator patch and ν is the percentage of the output mechanical power which is converted into flexural waves. At the considered frequency of excitation, ν is close to one for an actuator thickness of h=1mm (fig. 4.8).

An optimum geometry for maximum κ of the actuator patch was determined for zero bonding layer thickness. In fig. 4.14, the surface κ over length L and thickness h of the patch is represented by isovalue lines of constant κ. The optimum can be located at a thickness h^*=8mm and length L^*=170mm of the patch. It was first surprising, that an actuator of length 170mm should be ideally suited to excite a bending wave of wavelength 140mm. But considering the impressive thickness of the optimal sized actuator, the stiffening effect of the huge PZT patch in the laminate section leads to a wavelength of approximately twice the actuator length for the given frequency of excitation.

The capacitive and mechanical influence of a changing bonding layer thickness on the optimum geometry L^*, h^* was investigated. Assuming a conductive

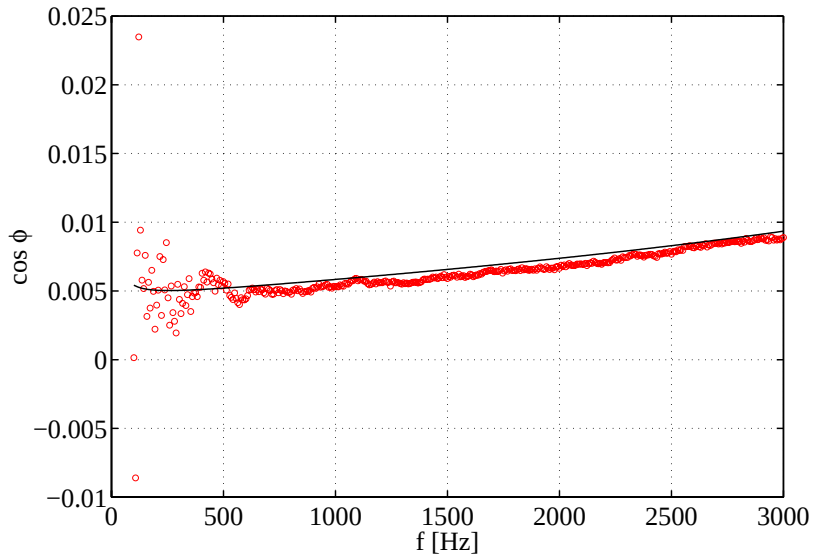

Figure 4.13: power factor $\cos\phi$: theory (—)and experiment (∘); h =8mm, H =3mm, $s = 2.5\mu$m

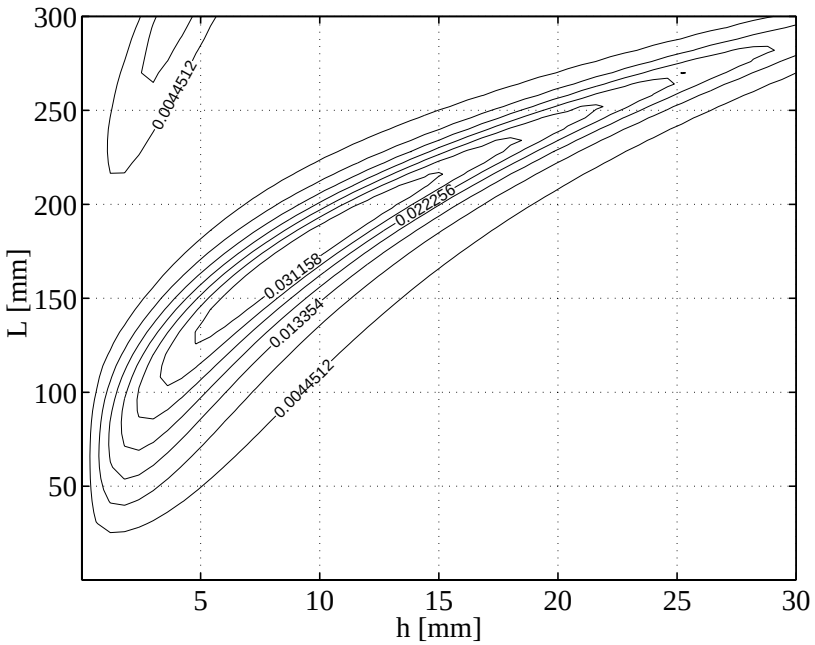

Figure 4.14: isovalues κ=const. over length L and thickness h of the PZT patch; f=1431Hz, PIC141 on steel beam, $s = 0$

conductive bonding layer			
s [μm]	L^* [mm]	h^* [mm]	κ
0	170	8	0,036
4	170	8	0,035
40	180	11	0,031
400	210	16	0,004

$s = 4\mu$m			
ε_r	L^* [mm]	h^* [mm]	κ
1	210	13	0,017
4	180	10	0,027
10	175	9	0,033
20	170	8	0,034

Table 4.3: influence of changing layer thickness s and relative permittivity ε_r on optimal geometry L^*, h^* and maximum effective bending power factor κ

bonding layer, the magnitude of the maximum κ and the corresponding geometry of the patch is given in table 4.3 for different bonding layer thicknesses. Also, for a constant bonding layer thickness of s=4μm, the maximum κ and L^*, h^* are listed for different relative dielectric permittivities ε_r of the bonding layer.

Presuming that bonding layer thicknesses of $s \leq$10μm can be achieved, the mechanical influence of the bonding layer on the optimal design and the resulting effective bending power factor is weak. The capacity of the bonding layer depends not only on the dielectric permittivity of the adhesive, but for a simple plate capacitor model also is inversely proportional to the thickness of the layer. Taking into consideration that the manufacturer's exact value for the relative permittivity ε_r of the adhesive is 2.75 and the assumed bonding layer thickness of s=4μm might be on the optimistically thin edge of the achievable range, it can be said that the capacitive influence of the bonding layer on the performance of the actuator, i.e. the maximum effective bending power factor is strong. The bonding layer should be as thin as possible and the permittivity of the layer and therefore the resulting capacity C_b should be high. In some applications it might be advised to use conductive epoxy for bonding, which eliminates any capacitive influence of the bonding layer. However, the cyanoacrylate adhesive used in the experiments gave satisfactory results if the actuator patches were firmly pressed against the substrate beam for the curing time.

Chapter 5

Discussion and Conclusion

5.1 Discussion of the results

Wang et al. [WDXC99] computed an 'electromechanical coupling coefficient' of a cantilevered piezoelectric bimorph[1)] actuator for different thickness ratios of substrate and PZT layer. The origin of the definition of this coupling coefficient remained somewhat unclear, still the resulting plots agree with figs. 4.3 and 4.2 and optimal thicknesses for the combination of PZT/steel and PZT/aluminum agree with results obtained from this work, whereas the computed coupling coefficients in the work of Wang et al. are smaller.

In experiments with cantilever bimorphs, Cunningham et al. [CJB97] determined the resonant amplitude of vibration for the first eigenmode of the cantilever for varying thicknesses of the substrate layer under constant voltage amplitude of excitation. The resulting amplitude of vibration at the free end of the cantilever exhibits the same dependence on the thickness ratio of the two layers as the EMCF in figs. 4.3 and 4.2. In particular, optimum thickness ratios for steel and aluminum substrate layers are comparable to the ones obtained from EMCF considerations in this work.

Strambi and Barboni [SBG95] computed the normalized curvature of a Bernoulli–Euler laminate, depending on the substrate to actuator thickness ratio. Their plotted results show close similarity to the corresponding curves for the EMCF, presented in figs. 4.3 and 4.2. Again, stiffer substrate materials lead to thicker piezoelectric layers for optimal curvature.

[1)] A bimorph is considered a laminated beam consisting of any two different layers extending over the entire length of the beam.

5.2 Conclusion

For piezoelectric bending actuators, an attempt was made to apply general criteria to optimize the piezoelectric layer thickness for best energy conversion. This attempt has been partially successful. It was shown, that the electromechanical coupling factor (EMCF) can be employed to determine optimal thicknesses and that these optimal values are independent of the prescribed deformation. Based on a quasi-static load cycle, the EMCF is a measure for the relative amount of the energy supplied to the system in one cycle, which is actually converted. This quasi-static load cycle is of hypothetical character and not a priori representative of the energy conversion in systems undergoing steady-state harmonic vibrations. It is the power factor $\cos\phi$, which gives the ratio of the converted to the maximally supplied energy in one harmonic cycle, and therefore can be considered the equivalent to the EMCF for steady-state vibration of electromechanical systems. Unlike it was the case for the EMCF, analytical expressions for an optimal thickness of the piezoelectric layer based on the actuator power factor could not be given. A model for a single piezoelectric actuator on an infinite beam was presented. Comparing numerical solutions to measured data obtained from an experimental setup, it was shown that this is a good model for the energy conversion in piezoelectric bending actuators. An optimal length and thickness for maximum power factor of the single actuator patch could be determined.

It is evident from both, the optimization for maximum EMCF and for maximum power factor in the case of the single actuator on the infinite beam, that the optimal thicknesses for the piezoelectric layer can be comparable to the thickness of the substrate layer, if the substrate material is stiff. Typical layer thicknesses in current technical applications are smaller. Of course, the thickness of the piezoelectric layer may also be limited by the strength of the material, as thicker layers will generally be expected to exhibit larger strains under similar deformation. However, if material strength is not a concern, current designs of piezoelectric layers for bending actuation should be reconsidered.

Bibliography

[Aul81] B.A. Auld: *Wave Propagation and Resonance in Piezoelectric Materials.* J. Acoust. Soc. Am, 70(6), 1577–1585, 1981.

[Aul89] B. A. Auld: *Acoustic Fields and Waves in Solids.* Krieger Publishing Company, 1989.

[BCJ] Don A. Berlincourt, Daniel R. Curran, Hans Jaffe: Piezoelectric and Piezomagnetic Materials and Their Function in Transducers, chapter 3.

[BSW95] H.T. Banks, R.C. Smith, Yun Wang: *The Modeling of Piezoceramic Patch Interactions with Shells, Plates and Beams.* Quarterly of Applied Mechanics, 53(2), 353–381, 1995.

[CA90] Edward F. Crawley, Eric H. Anderson: *Detailed Models of Piezoceramic Actuation of Beams.* Journal of Intelligent Material Systems and Structures, 1, 5–25, 1990.

[CdL87] Edward F. Crawley, Javier de Luis: *Use of Piezoelectric Actuators as Elements of Intelligent Structures.* AIAA Journal, 25(10), 1373–1385, 1987.

[CH88] L. Cremer, M. Heckl: *Structure-Borne Sound*, New York. Springer, 1988.

[CJB97] M.J. Cunningham, D.F.L. Jenkins, M.M. Bakush: *Experimental Investigation of Optimum Thickness of a Piezoelectric Element for Cantilever Actuation.* volume 144 671–681, 1997.

[CR94] Z. Chaudry, C.A. Rogers: *The Pin-Force Model Revisited.* Journal of Intelligent Material Systems and Structures, 5, 347–354, 1994.

[Fre97] Stephan Frese: *Electromechanical Coupling in Laminate Piezoceramic Beam Structures.* Master's thesis, Darmstadt University of Technology, Department of Applied Mechanics, 1997.

[GF92] Gary P. Gibbs, Chris R. Fuller: *Excitation of Thin Beams using Asymmetric Piezoelectric Actuators.* J. Acoust. Soc. Am., 6, 3221–3227, 1992.

[GUS89] V. T. Grinchenko, A. F. Ulitko, N. A. Shul'ga: *Mechanics of Coupled Fields in Elements of Structures, Vol 5: Electroelasticity (in Russian)*, Kiev. Naukova Dumka, 1989.

[HN68] Richard Holland, E.P. Eer Nisse: *Variational Evaluation of Admittances of Multielectroded Three-Dimensional Piezoelectric Structures.* IEEE Transactions on Sonics and Ultrasonics, SU-15(2), 119–132, 1968.

[HN69] R. Holland, E.P. Eer Nisse: *Design of Resonant Piezoelectric Devices*, Cambridge, Massachusetts. The M.I.T. Press, 1969.

[HPS+94] Craig L. Hom, Steven M. Pilgrim, Natarajan Shankar, Keith Bridger, Mona Massuda, Stephen R. Winzer: *Calculation of Quasi-Static Electromechanical Coupling Coefficients for Electrostrictive Ceramic Materials.* IEEE Transactions on Ultrasonics, Ferroelectrics and Frequency Control, 41(4), 542–551, 1994.

[Hun54] F.V. Hunt: *Electroacoustics*, New York. John Wiley & Sons, Inc., 1954.

[IEE78] *ANSI/IEEE Std. 176-1978: IEEE Standard on Piezoelectricity*, New York. The Institute of Electrical and Electronics Engineers, Inc., 1978.

[IEE88] *ANSI/IEEE Std. 176-1987: IEEE Standard on Piezoelectricity*, New York. The Institute of Electrical and Electronics Engineers, Inc., 1988.

[IRE58] *IRE Standards on Piezoelectric Crystals: Determination of the Elastic, Piezoelectric, and Dielectric Constants - The Electromechanical Coupling Factor, 1958.* volume 46 764–778, 1958.

[JCJ71] B. Jaffe, W. R. Cook, H. Jaffe: *Piezoelectric Ceramics*, Marietta, OH. R.A.N. Publishers, 1971.

[JS93] Franco Jona, G. Shirane: *Ferroelectric Crystals*, New York. Dover Publications, 1993.

[KJ91] S. J. Kim, J. D. Jones: *Optimal Design of Piezoactuators for Active Noise and Vibration Control*. AIAA Journal, 29(12), 2047–2053, 1991.

[Ler90] Reinhard Lerch: *Simulation of Piezoelectric Devices by Two- and Three-Dimensional Finite Elements*. IEEE Transactions on Ultrasonics, Ferroelectrics and Frequency Control, 37(2), 233–247, 1990.

[LP91] N. Lamberti, M. Pappalardo: *Computation of the Electromechanical Coupling Coefficient k in Piezoelectric Bounded Plates by Means of a Two-Dimensional Model*. Ultrasonics Symposium 1991, volume 1 621–624, 1991.

[LSR95] C. Liang, F.P. Sun, C.A. Rogers: *Determination of Design of Optimal Actuator Location and Configuration Based on Actuator Power Factor*. Journal of Intelligent Material Systems and Structures, 6, 456–464, 1995.

[LSR97] C. Liang, F.P. Sun, C.A. Rogers: *An Impedance Method for Dynamic Analysis of Active Material Systems*. Journal of Intelligent Material Systems and Structures, 8, 323–334, 1997.

[Mas50] Warren P. Mason: *Piezoelectric Crystals and Their Application to Ultrasonics*. D. Van Nostrand Company, Inc., 1950.

[Mau88] Gerard A. Maugin: *Continuum Mechanics of Electromagnetic Solids*, New York, volume 33 of *Applied Mathematics and Mechanics*. Elsevier Science Publishing Company, 1988.

[Ngu99] Minh Nam Nguyen: *Nichtlineares dynamisches Verhalten von Piezo-Balken-Systemen bei schwachem elektrischem Feld*. PhD thesis, Darmstadt University of Technology, 1999.

[Nis67] Errol P. Eer Nisse: *Variational Method for Electroelastic Vibration Analysis*. IEEE Transactions on Sonics and Ultrasonics, SU-14(4), 153–160, 1967.

[Rei96] Howard Reiss: *Methods of Thermodynamics*, Mineola, N.Y. 11501. Dover Publications, 1996.

[SBG95] Giulio Strambi, Renato Barboni, Paolo Gaudenzi: *Pin-Force and Euler-Bernoulli Models for Analysis of Intelligent Structures*. AIAA Journal, 33(9), 1746–1749, 1995.

[STÖ98] BORIS STÖBER: *Optimierung piezoelektrischer Aktuatoren zur Erzeugung von Biegeschwingungen.* Master's thesis, Darmstadt University of Technology, Department of Applied Mechanics, 1998.

[TIE68] H.F. TIERSTEN: *Natural Boundary and Initial Conditions from a Modification of Hamilton's Principle.* Journal of Mathematical Physics, 9(9), 1445–1451, 1968.

[TIE69] H. F. TIERSTEN: *Linear Piezoelectric Plate Vibrations*, New York. Plenum Press, 1969.

[ULI77] A.F. ULITKO: *Theory of Electromechanical Energy Conversion in Nonuniformly Deformable Piezoceramics.* Soviet Applied Mechanics; cover to cover translation of Prikladnaya Mekhanika 1055–1062, 1977.

[UTKN93] S. UEHA, Y. TOMIKAWA, M. KUROSAWA, N. NAKAMURA: *Ultrasonic Motors, Theory and Applications*, Oxford. Clarendon Press, 1993.

[VOI28] W. VOIGT: *Lehrbuch der Kristallphsik*, Leipzig. Teubner-Verlag, 1928.

[WAS68] K. WASHIZU: *Variational Methods in Elasticity and Plasticity*, Oxford. International Series of Monographs in Aeronautics and Astronautics. Pergamon Press, 1968.

[WDXC99] QUING-MING WANG, XIAO-HONG DU, BAOMIN XU, L. ERIC CROSS: *Electromechanical Coupling and Output Efficiency of Piezoelectric Bending Actuators.* IEEE Transactions on Ultrasonics, Ferroelectrics and Frequency Control, 46(3), 638–646, 1999.

[WFHS97] K. WOLF, S. FRESE, P. HAGEDORN, W. SEEMANN: *Thickness-Optimization of Piezoceramic Transducers for Energy Transfer.* Proceedings of DETC'97, 1997.

[ZR95] S. ZHOU, C. A. ROGERS: *Power Flow and Consumption in Piezoelectrically Actuated Structures.* AIAA Journal, 33, 1305–1311, 1995.

Lebenslauf

Kai-Dietrich Wolf
Karlstraße 30
65185 Wiesbaden

	-	Geboren am 29.03.68 in Wiesbaden
Mai	1987	Abiturprüfung an der Oranienschule in Wiesbaden
Okt	1988	Immatrikulation an der TUD, Fachbereich Maschinenbau
Jun	1991	Abschluß des Vordiploms Maschinenbau
Okt	1991	Wechsel in den Fachbereich Mechanik
Aug	1992	Integriertes Auslandsstudium an der 'University of California', Berkeley (1 Jahr)
Sep	1994	Abschlußprüfung Mechanik
seit Okt	1994	Wissenschaftlicher Mitarbeiter am Fachbereich Mechanik, AG Dynamik der Technischen Universität Darmstadt